DNA sequence differences and temperature are determinants of meiotic recombination outcome

Simon D. Brown[1,3], Mimi N. Asogwa[1], Marie Jézéquel[1], Charlotte Audoynaud[1,4], Samantha J. Mpaulo[1], Matthew C. Whitby[2], and Alexander Lorenz[1,*]

[1]The Institute of Medical Sciences (IMS), University of Aberdeen, Foresterhill, Aberdeen AB25 2ZD, UK

[2]Department of Biochemistry, University of Oxford, South Parks Road, Oxford OX1 3QU, UK

[3]Present address: MRC Institute of Genetics & Molecular Medicine, University of Edinburgh, Edinburgh EH4 2XU, UK

[4]Present address: Institut Curie, PSL Research University, UMR3348-CNRS, 91405 Orsay, France

*Correspondence should be addressed to
Alexander Lorenz
Institute of Medical Sciences (IMS)
University of Aberdeen
Foresterhill
Aberdeen AB25 2ZD
United Kingdom
Phone: +44 1224 437323
E-mail: a.lorenz@abdn.ac.uk

Abstract

Meiotic recombination is essential for producing healthy gametes, and also generates genetic diversity. DNA double-strand break (DSB) formation is the initiating step of meiotic recombination, producing, among other outcomes, crossovers between homologous chromosomes, which provide physical links to guide accurate chromosome segregation. The parameters influencing DSB position and repair are thus crucial determinants of reproductive success and genetic diversity. Using *Schizosaccharomyces pombe*, we show that the distance between sequence polymorphisms across homologous chromosomes has a strong impact on recombination, not only locally as intragenic events, but also on crossover frequency. This effect is controlled by MutS-MutL factors and DNA helicases. Additionally, we establish temperature as a major factor modulating meiotic recombination frequency, and identify DSB processing as a temperature-sensitive step in the meiotic recombination pathway. This exposes a complex interplay of genetic and environmental parameters shaping the outcome of meiotic recombination.

2

Introduction

Correct chromosome segregation during meiosis depends on pairing and physical connection of homologous chromosomes (homologs). Physical connections are established by the repair of programmed DNA double-strand breaks (DSBs) using the homolog rather than the sister chromatid as a template (i.e. interhomolog recombination) and by ensuring that interhomolog recombination intermediates are processed into crossovers (COs). The formation of DSBs by the transesterase Spo11 is thus a key step in initiating recombination during meiosis (Lam and Keeney 2015). Regions of high-frequency Spo11 recruitment, and thus DSB formation, are called hotspots (Wahls and Davidson 2012). One of the best characterized category of hotspots are cAMP-responsive elements, such as the *ade6-M26* hotspot and its derivatives in *Schizosaccharomyces pombe*, created by point mutations in the *ade6* gene (Wahls and Davidson 2012). *M26*-like hotspots are defined by the DNA sequence heptamer 5'-ATGACGT-3', which represents the core of a binding site for the Atf1-Pcr1 transcription factor (Kon et al. 1997). Although binding of Atf1-Pcr1 and associated transcription already creates open chromatin at *M26*-like hotspots (Kon et al. 1997; Yamada et al. 2017), a very high frequency of meiotic recombination requires a conducive chromatin environment in a wider genomic context (Steiner and Smith 2005; Yamada, Ohta, and Yamada 2013). This network of parameters determines the overall level of DSB formation at a given genomic locus.

Following break formation, DSB ends are resected to initiate homologous recombination, which during meiosis follows either a Holliday junction/D-loop resolution or a synthesis-dependent strand annealing pathway (Lam and Keeney 2015; Hunter 2015). As a repair template, the sister chromatid or the homolog will be used (Humphryes and Hochwagen 2014). Based on this, it has been suggested that the governance of meiotic recombination could be viewed as a two-tiered decision system (Lorenz 2017). The first decision being template choice (interhomolog vs. intersister recombination), and the second being how the recombination intermediate is resolved - i.e. the CO/non-crossover (NCO) decision. The template choice decision is mainly driven by meiosis-specific factors of the chromosome axis and by the meiotic recombinase Dmc1 supported by its mediators (Humphryes and Hochwagen 2014). In budding yeast there is a basic understanding of how the interhomolog bias is established, although some mechanistic details still remain to be elucidated (Hong et al. 2013). Since homologs are not necessarily identical on a DNA sequence level, a DSB end invading the homolog for repair can generate a mismatch-containing heteroduplex DNA. Mismatches can be corrected by the mismatch repair system, consisting of the highly conserved MutS and MutL proteins (Surtees, Argueso, and Alani 2004). Additionally, the MutS-MutL complex can also block strand invasion to avoid recombination between non-homologous sequences (Surtees, Argueso, and Alani 2004). The CO/NCO-decision happens as the next step; here the decision is taken whether an already established interhomolog recombination intermediate is processed into a CO or a NCO. Determinants of the CO/NCO-decision are less well studied, but the DNA helicase/translocase FANCM (Fml1 in *Sz. pombe*) has been shown to limit CO formation in fission yeast and *Arabidopsis* (Lorenz et al. 2012; Crismani et al. 2012). RecQ-type DNA helicases perform a wide range of regulatory roles in homologous recombination, and one of them probably is the promotion of NCO formation during meiosis in various organisms (De Muyt et al. 2012; Lukaszewicz, Howard-Till, and Loidl 2013; Hatkevich et al. 2017).

In addition to these intrinsic genetic determinants, environmental factors play a role in dictating the outcome and dynamics of meiotic recombination. Environmental temperature has been identified as a modulating factor of meiotic recombination frequency in organisms incapable of regulating their body temperature (Bomblies, Higgins, and Yant 2015). The laboratory model yeasts *Sz. pombe* and *Saccharomyces cerevisiae* are globally distributed species with a poorly understood ecology (Liti 2015; Jeffares 2018), but it is likely that they are exposed to changing temperatures in their respective niches. Although a few observations about environmental temperature altering meiotic recombination have been made in the past in a variety of organisms, including yeasts (Plough

91 1917; Rose and Baillie 1979; Börner, Kleckner, and Hunter 2004; Pryce et al. 2005; Higgins et al.
92 2012), only recently more systematic approaches have explored the effect of the full temperature
93 range at which meiosis is possible on meiotic recombination in a particular organism (Zhang et al.
94 2017; Lloyd et al. 2018; Modliszewski et al. 2018).
95   Here, we employ a series of genetic recombination assays featuring intragenic markers at
96 differently sized intragenic intervals and flanking intergenic markers to identify and characterize
97 intrinsic determinants of template choice and CO/NCO-decision in fission yeast. We show that the
98 relative positions of DNA sequence polymorhisms between homologs have a strong impact on
99 recombination outcome, not only locally in the form of intragenic recombination, but also on the CO
100 frequency between an up- and a downstream marker. The anti-recombinogenic activity of MutS-
101 MutL factors, and of the DNA helicases Fml1 and Rqh1 modulate recombination outcome
102 differentially when comparing various intragenic intervals. Furthermore, we provide evidence how a
103 simple environmental factor, such as temperature, influences recombination outcome locally, and
104 identify DSB processing as the likely temperature-sensitive step of meiotic recombination.
105
106

107 # Results
108 ## Rationale of the meiotic recombination assay
109 Our genetic recombination assay features intragenic markers (point mutations in the *ade6* gene) and
110 flanking intergenic markers (*his3*[+]-*aim* and *ura4*[+]-*aim2*) (Figure 1A-B). This assay allows us to
111 monitor various recombination outcomes: (I) intragenic recombination events producing *ade6*[+]
112 recombinants, (II) crossovers (COs) between the flanking intergenic markers (*his3*[+]-*aim* and *ura4*[+]-
113 *aim2*), and (III) the ratio of COs vs. non-crossovers (NCOs) among intragenic *ade6*[+] recombination
114 events (Figure 1A). Changes in intragenic recombination and overall CO frequencies observed in
115 this assay can be explained by an altered frequency of DSB formation at a given *ade6* mutant allele,
116 or a change in repair template usage. The percentage of COs and NCOs among intragenic *ade6*[+]
117 recombination events is the genetic readout for the CO/NCO-decision, representing recombination
118 intermediate processing after successful strand exchange between homologs. These events can be
119 the result of gene conversions associated with COs or NCOs (non-reciprocal exchange of hereditary
120 information), or of intragenic COs as a result of recombination intermediate resolution between the
121 two point mutations within *ade6* (reciprocal event) (Figure 1A, Figure 1-figure supplement 1; see
122 below for details).
123

124 ## The physical distance between point mutations of heteroalleles defines the frequency of
125 ## intragenic recombination events and their associated CO/NCO ratio
126 Apart from absolute DSB levels, intragenic recombination frequency is also influenced by the
127 distance between point mutations in a given chromosomal region (Gutz 1971; Zahn-Zabal and Kohli
128 1996; Fox et al. 1997; Steiner and Smith 2005). Intragenic recombination in our assays (Figure 1A)
129 has so far been monitored using point mutations within the *ade6* coding sequence, which are at least
130 1kb apart (Osman et al. 2003; Lorenz, West, and Whitby 2010; Lorenz et al. 2012). We wondered
131 whether the level of COs among intragenic recombination events also changes, when the distance
132 between point mutations was decreased. Therefore, we selected a series of point mutations, which
133 cover almost the complete length of the *ade6* coding sequence (Figure 1B, Figure 1-table
134 supplement 2). These point mutants include the strong meiotic recombination hotspots *ade6-M26*, -
135 *3074*, *-3083*, at the 5' end of the gene and *-3049* at the 3' prime end of the gene, as well as the weak
136 hotspot *ade6-M375*, and the non-hotspot alleles *ade6-M216*, *-704*, *-52*, *-149*, *-51*, and *-469* (Figure
137 1B, Figure 1-table supplement 2). All strong hotspots mimic a cAMP-response element/Atf1-Pcr1
138 binding site (Kon et al. 1997; Steiner and Smith 2005). It can be safely assumed that a given hotspot
139 will receive the same amount of breakage independent of the *ade6* allele present on the homolog.

4

140 This means that the differences seen in the combinations of one specific hotspot with various *ade6*
141 alleles will depend on processes downstream of DSB formation. Indeed, the frequency of intragenic
142 recombination positively correlates with the distance between the *ade6* alleles, when the same
143 hotspot is used (Figure 1C, black and grey lines). The weak hotspot allele *ade6-M375*, which is at a
144 similar position as the strong hotspot alleles *ade6-3074* & *ade6-3083*, induces recombination only
145 moderately. However, intragenic recombination frequency at *ade6-M375* shows a similar correlation
146 with respect to distance between the DNA polymorphisms (Figure 1C, green line). Intragenic
147 intervals of similar size containing the meiotic recombination hotspot alleles, *ade6-3083*, *ade6-3074*,
148 or *ade6-3049*, and a non-hotspot allele produce equivalent intragenic recombination levels (Figure
149 1C). Therefore, these hotspot alleles behave similarly in determining intragenic recombination
150 frequency. Intriguingly, these observations are also largely true for CO frequency among intragenic
151 recombination events. The shorter an intragenic distance between polymorphisms is, the more likely
152 an intragenic recombination event is resolved as a NCO (Figure 1D). For crosses involving the
153 hotspot alleles *ade6-3083* or *ade6-3074* the effect apparently tails off at intragenic distances >600bp
154 (Figure 1D). Combining hotspot alleles on both homologs within a cross results in increased overall
155 intragenic recombination rate compared with hotspot × non-hotspot crosses (Figure 1E), similar to
156 what was previously reported (Hyppa and Smith 2010). However, there is no notable increase in
157 COs among intragenic recombination events when compared to hotspot × non-hotspot crosses with
158 similar intragenic distance between point mutations (Figure 1F). This indicates that the frequency of
159 CO among intragenic recombination events is a function of the distance between the *ade6*
160 heteroalleles on the homologs. The distribution of different NCO/CO classes amongst intragenic
161 recombination events follows a pattern consistent with intragenic NCOs events more likely being
162 associated with the hotter allele. This means that the allele more likely to receive a DSB is the
163 recipient of genetic information in the overwhelming majority of cases, which might represent a *bona*
164 *fide* gene conversion (Figure 1G). If comparable hotspots are combined in a cross the two intragenic
165 NCO classes occur with roughly equal frequency (Figure 1G, compare cross *ade6-3083×ade6-3049*
166 to crosses *ade6-3083×ade6-469* & *ade6-M375×ade6-3049*).

167 The observed distribution patterns also suggest that, at these long intragenic intervals, a
168 subset of CO events could stem from the processing of one joint molecule, presumably a single
169 Holliday junction (Cromie et al. 2006) or its precursors, positioned between the two *ade6* point
170 mutations, in contrast to a gene conversion event being resolved as a CO. This hypothesis makes
171 the following prediction: If CO events among Ade+ recombinants (mostly Ura- His- genotypes) are
172 created by processing of a joint molecule situated between the two *ade6* point mutations, then
173 reciprocal Ade- Ura+ His+ recombinants carrying the mutations of both *ade6* heteroalleles must
174 exist. To test this, we sequenced the *ade6* locus from 32 Ade- Ura+ His+ colonies from an *ade6-*
175 *3083×ade6-469* cross. Based on the frequency of 0.677% Ade+ Ura- His- events among the total
176 viable progeny in such a cross representing 8.375% of recombinants among all Ura- His- colonies
177 (240 Ura- His- colonies among 2,969 total viable progeny, 8.083%), we would expect that 2-3 of the
178 32 Ade- Ura+ His+ carry both the *3083* and the *469* mutation within the *ade6* locus, if all events were
179 generated by CO processing of a recombination event between the two heteroalleles. Indeed, we
180 observed 2 instances in which the *ade6* locus of Ade- Ura+ His+ progeny harbored both mutations
181 (Figure 1-figure supplement 1), supporting the existence of intragenic COs (Figure 1A).

182

183 **MutSα and MutLα are strong negative modulators of recombination frequency specifically at**
184 **short intragenic intervals**
185 Potential candidates for genetic pathways modulating recombination frequency at intragenic
186 intervals of different lengths are MutS-MutL complexes which bind to heteroduplex DNA and repair
187 mismatches (Surtees, Argueso, and Alani 2004). *Sz. pombe* has a streamlined nuclear mismatch
188 repair system consisting of MutSα (Msh2-Msh6), MutSβ (Msh2-Msh3), and a single MutL (MutLα,
189 Mhl1-Pms1); there is also a mitochondrial MutS protein called Msh1 (Marti, Kunz, and Fleck 2002).

190 Importantly, the meiotic pro-crossover factors MutSγ (Msh4-Msh5), the meiosis-specific MutLγ
191 component Mlh3, and Mlh2 – a MutLβ-homolog and a modulator of meiotic gene conversion tract
192 length – are all missing in fission yeast (Manhart and Alani 2016; Duroc et al. 2017). This suggests
193 that *Sz. pombe* is a suitable model to study the role of MutSα/β-MutLα during meiosis without
194 potential crosstalk from MutSγ-MutLγ pro-crossover factors (Rogacheva et al. 2014).

195 At small intragenic intervals the absence of MutSα-MutLα causes a substantial increase in
196 intragenic recombination frequency (Figure 2A, Figure 2-figure supplement 1). This relationship
197 shows an inverse correlation, i.e. the shorter the intragenic interval the higher the increase. This
198 ranges from a ~70-fold increase at the *ade6-149×ade6-3049* (33bp) interval, via a ~35-fold one at
199 *ade6-3049×ade6-51* (53bp), to a ~10-fold augmentation at the *ade6-M216×ade6-3083* (85bp)
200 interval (Figure 2A, Figure 2-figure supplement 1). The MutSα mutants (*msh2-30*, *msh6Δ*) and the
201 MutLα mutants (*mlh1Δ*, *pms1-16*) displayed similar frequencies of intragenic recombination to each
202 other, and the *msh2-30 mlh1Δ* double mutant is not discernible from either single mutant (Figure
203 2A), indicating that MutSα and MutLα work in the same pathway. Deleting MutSβ (*msh3*) is of no
204 consequence at the *ade6-M216×ade6-3083* interval (Figure 2A; *p*=0.613 against wild type, two-tailed
205 Mann-Whitney U), likely because all the *ade6* mutations tested are substitution mutations, and
206 MutSβ only recognizes insertion/deletion loop mismatches larger than 2 nucleotides (Surtees,
207 Argueso, and Alani 2004). At larger intragenic intervals, there seems to be little or no role for MutSα-
208 MutLα in limiting recombination events. In fact, a moderate, but mostly non-significant, tendency of
209 lower intragenic recombination frequency can be observed (Figure 2B, Figure 2-figure supplement
210 1). Altogether, these data show that MutSα-MutLα has a strong anti-recombinogenic role at small
211 intragenic intervals, but seemingly no role in determining recombination outcome at large intragenic
212 intervals.

213 Mutating *mutSα-mutLα* genes increases CO frequency among intragenic recombination
214 events (Figure 2C-D, Figure 2-figure supplement 2) and/or changes the distribution of recombinant
215 classes (Figure 2-figure supplement 3). Both long and short intragenic intervals involving the *ade6-*
216 *3083* allele showed increases in associated CO frequency in comparison to wild type, albeit this
217 trend was not statistically significant in all cases (Figure 2C-D, Figure 2-figure supplement 2). This
218 trend makes the share of COs among intragenic recombination events independent of the length of
219 the interval (compare Figure 1D with Figure 2C-D, Figure 2-figure supplement 2). Interestingly, there
220 is also a substantial shift in CO classes among intragenic recombination events from mostly *ura⁻ his⁻*
221 to mainly *ura⁺ his⁺* in *mutSα-mutLα* mutants at the short *ade6-M216×ade6-3083* interval (Figure 2-
222 figure supplement 3). This is not a consequence of selective survival or the formation of diploid or
223 disomic spores, because *mutSα-mutLα* mutants have a spore viability similar to wild type, and the
224 extent of the phenotype is the same in several different mutants (Supplementary File 1-Table S2).
225 The possible significance of this finding is considered in the Discussion. As with intragenic
226 recombination frequency, the *mutSβ* deletion *msh3Δ* behaves just like wild type for CO outcome
227 (Figure 2C-D; *p*=0.439 against wild type, two-tailed Mann-Whitney U).

228

229 **Fml1 is a negative modulator of intragenic CO frequency independent of the distance**
230 **between point mutations**
231 The DNA helicases, Fml1 and Rqh1, are also prime candidates for modulating recombination
232 frequency at intragenic intervals of different lengths (Lorenz et al. 2012; Cromie, Hyppa, and Smith
233 2008). However, Fml1 apparently does not modulate intragenic recombination levels, as at all
234 intragenic intervals tested, *fml1Δ* is similar to wild type (Figure 3A-B, Figure 3-figure supplement 1A).
235 In contrast, the RecQ-family DNA helicase Rqh1 is required for wild-type levels of intragenic
236 recombination (Lorenz et al. 2012). The deletion of *rqh1* reduces intragenic recombination frequency
237 to about a third of wild-type percentage at short (*ade6-M216×ade6-3083*, *ade6-3049×ade6-469*)

6

238 intervals, and to about a tenth of wild-type frequency at the long *ade6-3083×ade6-469* interval
239 (Figure 3A-B, Figure 3-figure supplement 1).
240   As with long intervals (Lorenz et al. 2012) *fml1Δ* results in a ~10 percentage point increase of
241 CO frequency among intragenic recombination events at short intervals (Figure 3C-D, Figure 3-figure
242 supplement 1). The absence of Rqh1 induces moderate increases in CO levels among intragenic
243 recombination events at the 85bp *ade6-M216×ade6-3083* and the 1,3520bp *ade6-3083×ade6-469*
244 interval, which are not statistically significant (Figure 3C-D). However, at the 254bp *ade6-*
245 *3049×ade6-469* interval CO frequency among *ade6+* events is raised by 17 percentage points in
246 *rqh1Δ* (p=3.72×10^{-9} against wild type, two-tailed Mann-Whitney U) (Figure 3-figure supplement 1).
247 Because *ade6-3083* is a more complex allele than *ade6-3049* (see Discussion), this potentially
248 indicates that Fml1 can drive NCO pathway(s) independently of the complexity of the underlying
249 DNA sequence, whereas Rqh1 can fulfill this role only at simple *ade6* alleles with a single substitution
250 mutation. Overall, these data show that Fml1 has no role in modulating intragenic recombination
251 levels, but drives NCO formation downstream after successful strand invasion and DNA synthesis.
252 Rqh1 promotes intragenic recombination, but also has moderate anti-recombinogenic activity in CO
253 formation among intragenic recombination events.
254
255 **The "fertile range" of fission yeast lies between 11°C and 33°C**
256 Bomblies and coworkers recently noted that to understand the extent to which temperature affects
257 meiotic recombination, it is important to know the "fertile range" of the tested species; otherwise the
258 results will be skewed by including temperatures outside the "fertile range" or omitting temperatures
259 within it (Lloyd et al. 2018). We set up matings of prototrophic fission yeast strains (ALP714×ALP688)
260 in a temperature range between +4°C and +35°C on sporulation media. Matings were checked
261 regularly until asci containing spores were observed, or, if not, the experiment was abandoned after
262 30 days. No asci were observed at +4°C and at +35°C after one month of incubation, putting the
263 "fertile range" of *Sz. pombe* somewhere between these two temperatures. Indeed, mating at 11°C
264 resulted in the formation of asci containing spores within 2 weeks, at 16°C within 1 week, at 20°C
265 within 5 days, at 25°C and 30°C within 3 days, and at 33°C within 2 days. Sporulation efficiency was
266 calculated as the percentage of asci containing spores in a given population of cells after the
267 indicated time at each temperature. Sporulation efficiency was ~25% at all temperatures, except at
268 11°C when it was only ~5% (Figure 4A).
269   During the following meiotic recombination assays performed at 11°C, 16°C, 20°C, 25°C,
270 30°C and 33°C ("fertile range"), we also monitored spore viability by random spore analysis. At all
271 temperatures tested, spore viability was ~60% (Figure 4B), indicating that at 11°C when sporulation
272 is comparably inefficient (Figure 4A), the spores that developed did not suffer from decreased
273 viability.
274
275 **Meiotic intragenic recombination levels vary greatly within the "fertile range"**
276 To assess whether temperature alters meiotic recombination outcome, assays were performed at
277 temperatures within the "fertile range". We tested five different combinations of *ade6* heteroalleles:
278 two large intragenic intervals containing a strong hotspot allele (*ade6-3083×ade6-469*, 1,320bp &
279 *ade6-M216×ade6-3049*, 1,168bp), one large intragenic interval containing a weak hotspot allele
280 (*ade6-M375×ade6-469*, 1,335bp), and two small intragenic intervals containing a strong hotspot
281 allele (*ade6-M216×ade6-3083*, 85bp & *ade6-3049×ade6-469*, 254bp). The frequency of intragenic
282 recombination is considerably lower at colder temperatures (11°C, 16°C and 20°C), and tends to
283 plateau between 25°C and 33°C (Figure 4C-E). One of the large intervals (*ade6-3083×ade6-469*)
284 displayed a distinct peak at 30°C (p=2.67×10^{-11} 25°C vs. 30°C, p=2.6×10^{-5} 30°C vs. 33°C; two-tailed
285 Mann-Whitney U test). Intriguingly, the fold-change in intragenic recombination frequency between
286 16°C (lowest temperature tested in all intervals) and the temperature producing the highest
287 intragenic recombination frequency is substantially lower in the cross with the weak *ade6-M375*

288 hotspot (2.7-fold) than in the crosses containing a strong hotspot allele (5-fold to 11-fold)
289 (Supplementary File 1-Table S4). This also holds true if intragenic recombination frequency is
290 compared between 16°C and 25°C (the mating temperature generally used for this type of
291 experiment): 2.4-fold change in *ade6-M375×ade6-469* vs. a 4.3- to 6.6-fold change in the crosses
292 containing a strong hotspot allele (Supplementary File 1-Table S4). The very short *ade6-*
293 *M216×ade6-3083* intragenic interval (85bp) shows a stronger fold-change over temperature (6.6-
294 fold at 16°C vs. 25°C), than the longer intervals containing a hotspot allele (254bp – 1,320bp; 4.3-
295 to 4.8-fold at 16°C vs. 25°C) (Supplementary File 1-Table S4). This suggests, (I) that, as a general
296 trend, lower temperatures reduce the frequency of intragenic recombination regardless of physical
297 distance between *ade6* mutations, (II) that intragenic recombination at weak hotspots is less
298 sensitive to temperature changes than intragenic recombination at strong hotspots, and (III) that
299 intragenic recombination at very short intervals is singularly susceptible to temperature changes.
300

301 **Meiotic CO frequency varies moderately within the "fertile range"**
302 Given that major changes in intragenic recombination levels are observed across temperatures, we
303 were surprised to find that overall CO levels and CO frequencies among intragenic events were less
304 sensitive to temperature changes. The frequency of COs between *ura4+-aim2* and *his3+-aim* are
305 not substantially altered as crossing temperature changes (Figure 4-figure supplement 1). In all
306 intervals tested CO frequency in the total population is only significantly lower at the temperatures
307 of 11°C and 16°C, but then plateaus at 20°C and higher (Figure 4-figure supplement 1A-C; Tukey's
308 Honest Significant Differences). CO frequency among intragenic *ade6+* events was even more stable
309 with temperature changes. The weak hotspot cross *ade6-M375×ade6-469* was completely unfazed
310 by temperature changes (*p*=0.314, Kruskal-Wallis test). The crosses at cold temperatures (11°C,
311 16°C & 20°C) in all the other intervals displayed a moderate tendency to higher CO percentages
312 than crosses at 30°C or 33°C (Figure 4-figure supplement 1; Tukey's Honest Significant Differences).
313 The latter observation could indicate a mechanism like CO homeostasis at work (Martini et al. 2006;
314 Kan, Davidson, and Wahls 2011).
315

316 **Meiotic DSB levels do not appear to change with temperature**
317 Following the observation that temperature modulates meiotic recombination outcome, we next
318 sought to pinpoint which specific steps during meiotic recombination are sensitive to temperature
319 changes. Therefore, we assessed whether DSB formation is likely disturbed using the cytological
320 markers Rec7-GFP and Rad11-GFP. Rec7 (Rec114 in *S. cerevisiae*), one of the co-factors essential
321 for Spo11 recruitment and function (Miyoshi, Ito, and Ohta 2013), can be detected on meiotic
322 chromatin and is considered a marker for DSB initiation sites (Lorenz et al. 2006). As part of RPA
323 (replication protein A) Rad11 becomes associated with the single-stranded DNA exposed by strand
324 resection following removal of Spo11, and is thus a marker for DSB formation (Parker et al. 1997).
325 Rec7- and Rad11-focus numbers enable us to assess meiotic DSB levels indirectly. For Rec7- and
326 Rad11-focus counts, linear elements outlined by myc-tagged Hop1 were used to identify meiotic
327 prophase I nuclei in chromatin spreads from meiotic time-courses (Lorenz et al. 2004; Brown,
328 Jarosinska, and Lorenz 2018; Loidl and Lorenz 2009). We chose to perform these experiments at
329 the extreme temperatures of the "fertile range" (16°C and 33°C), which were still producing high
330 sporulation efficiency and significantly different recombination frequencies (Figure 4).
331 Based on previous observations that recombination markers are most abundant in the thread
332 and network stage of linear element formation (Lorenz et al. 2006), we selectively counted foci at
333 these stages. On average between ~16 foci of both Rec7-GFP and Rad11-GFP per nucleus were
334 observed at 16°C and 33°C (Figure 5A-B). The Rec7-GFP focus count was actually somewhat higher
335 at the lower temperature (18.2 at 16°C vs. 14.1 at 33°C, *p*=0.0017, two-tailed Mann-Whitney U test),
336 whereas the Rad11-GFP focus numbers were indiscernible between 16°C (15.9 foci/nucleus) and
337 33°C (16.2 foci/nucleus) (Supplementary File 1-Table S5; *p*=0.794, two-tailed Mann-Whitney U test).

338 These experiments suggest that overall DSB formation is largely unaltered between 16°C
339 and 33°C, because any subtle changes observed are unlikely to explain the lowered recombination
340 frequencies at cold temperatures.
341

342 **Processing of DSBs is potentially altered by temperature**
343 Rqh1 and Exo1 function in long-range strand resection in mitotic and meiotic cells in fission yeast
344 (Langerak et al. 2011; Osman et al. 2016). Sfr1 forms a complex with Swi5 to support strand
345 exchange, thereby promoting meiotic recombination (Haruta et al. 2006; Lorenz et al. 2012). Less
346 efficient DSB processing and/or strand exchange could potentially explain why recombination levels
347 are reduced at colder temperatures. The expectation would be that mutants defective in strand
348 resection or strand exchange would be more sensitive to temperature changes than wild type (i.e.,
349 a synergistic effect of mutational and environmental weakening of these processes). Therefore,
350 meiotic recombination outcome in *ade6-3083×ade6-469* crosses of *rqh1Δ*, *exo1Δ*, and *sfr1Δ* single
351 mutants performed at 16°C and 25°C was determined. The fold difference in intragenic
352 recombination frequency between 16°C and 25°C for wild type and each deletion was calculated to
353 assess whether the reduction in intragenic recombination at cold temperatures is epistatic or
354 synergistic with deleting *rqh1*, *exo1*, or *sfr1*. In wild-type crosses intragenic recombination is 4.3-fold
355 lower at 16°C compared to 25°C ($p=6.428×10^{-12}$, two-tailed Mann-Whitney U test). However, in
356 *rqh1Δ*, *exo1Δ*, and *sfr1Δ* crosses intragenic recombination levels are 7.2-fold ($p=1.402×10^{-9}$, two-
357 tailed Mann-Whitney U test), 7.1-fold ($p=4.665×10^{-11}$, two-tailed Mann-Whitney U test), and 7.9-fold
358 ($p=6.265×10^{-7}$, two-tailed Mann-Whitney U test) lower at 16°C than at 25°C, respectively (Figure 6).
359 The fold changes in overall CO frequency and CO levels among *ade6*[+] recombinants are largely
360 unchanged or do not follow an obvious pattern (Supplementary File 1-Table S4). Long-range strand
361 resection and the action of strand exchange factors are potentially important for maintaining
362 intragenic recombination frequency especially at colder temperatures, indicating that these
363 processes possibly are temperature-sensitive.
364

365 # Discussion
366 **Differences in the DNA sequences of the homologs affect recombination**
367 We used a genetic recombination assay with *ade6* as central marker gene to determine whether
368 different distances between polymorphisms (intragenic interval) influence intragenic and intergenic
369 recombination outcome (Figure 1). This potentially has implications for how we think about meiotic
370 recombination. Rather than simple gene conversions at single loci, which are thought to primarily
371 arise from mismatch repair or from DNA synthesis during DSB repair (Holliday 2007), intragenic
372 recombination events involving two distinct point mutations on the homologs have the additional
373 possibility of being caused by intragenic COs (Figure 1-figure supplement 1). This would imply that
374 the occurrence of a CO between two point mutations is more likely the longer the distance between
375 the two heteroalleles is, and that this will result in an intragenic event with a higher probability. This,
376 admittedly, exposes a rather blurred boundary between what constitutes a bifactorial GC event
377 associated with a CO and what an intragenic CO event. The three mechanisms of GC formation
378 (mismatch repair, DNA synthesis during DSB repair, and intragenic COs) are not mutually exclusive,
379 but to a degree even presuppose each other.
380 The observed effects for different parental and recombinant classes amongst progeny having
381 undergone a meiotic intragenic recombination event can be explained by envisioning a DSB 5' or 3'
382 of a point mutation leading to a recombination intermediate (D-loop, Holliday junction), which will
383 then be processed immediately at the break site, or ends up somewhat removed from the initial
384 break site by multiple consecutive invasion steps, by branch migration, or both (Farah, Cromie, and
385 Smith 2009; Piazza, Wright, and Heyer 2017; Marsolier-Kergoat et al. 2018). The genetic makeup
386 of the progeny is, therefore, a compound result of processing distinct recombination intermediates

9

387 in different ways. The genetic composition of wild-type and mutant progeny resulting from the meiotic
388 recombination assays can be explained as different combinations of scenarios suggested previously
389 (Lorenz et al. 2014). For example, recombination between *ade6-3083* and *ade6-M216*, which gives
390 rise to mainly Ade⁺ His⁺ Ura⁻ NCOs and Ade⁺ His⁻ Ura⁻ COs, may be explained by the model in Figure
391 7A. In this model, a bias in favour of Ade⁺ His⁻ Ura⁻ COs stems from strand exchange/branch
392 migration being constrained to within the region defined by the *ade6-3083 – ade6-M216* interval and
393 resolution of the recombination intermediate occurring by D-loop cleavage (Figure 7A, C). Ade⁺ His⁺
394 Ura⁻ NCOs and additional Ade⁺ His⁻ Ura⁻ COs come from HJ resolution (Figure 7A, C). However,
395 certain mutant situations can dramatically alter the outcome, e.g. recombination at *ade6-*
396 *M216×ade6-3083* in *mutSα-mutLα* mutants leads to relatively few Ade⁺ His⁻ Ura⁻ COs and a big
397 increase in the proportion of Ade⁺ His⁺ Ura⁺ COs (Figure 2, Figure 2-figure supplement 3). We
398 considered whether this might have something to do with the complexity of the *ade6-3083* allele,
399 which consists of multiple substitution mutations and can potentially form a C/C-mismatch in the
400 heteroduplex DNA during strand exchange that is less efficiently repaired during meiosis than other
401 mismatches (Schär and Kohli 1993). However, a moderate shift of CO recombinant classes among
402 intragenic events can also be seen at the small *ade6-149×ade6-3049* interval (Figure 2-figure
403 supplement 3). Unlike *ade6-3083*, *ade6-3049* contains only a single nucleotide difference (Figure 1-
404 table supplement 2) and, therefore, the complexity of a given *ade6* allele is unlikely to be the critical
405 factor affecting the shift in CO recombinant class. Instead, we think that a deficit in heteroduplex
406 rejection and mismatch repair, caused by loss of *msh2*, could result in strand exchange/branch
407 migration extending beyond the non-hotspot mutation (i.e. *ade6-M216* or *ade6-149*) prior to D-loop
408 cleavage/HJ resolution, and the base-pair mismatches in the recombinant chromosomes remaining
409 unrepaired. Together, these altered features could explain the increase in Ade⁺ His⁺ Ura⁺ COs at the
410 *ade6-M216×ade6-3083* and *ade6-149×ade6-3049* intervals in *mutSα-mutLα* mutant crosses (Figure
411 7B, C).

412   Recombination outcome in a *msh2Δ* in *S. cerevisiae* has also been shown to be more
413 complex than in wild type (Martini et al. 2011; Cooper et al. 2018). Intriguingly, in *S. cerevisiae* the
414 action of Msh2 seems to be restricted to class I COs, which are subjected to CO interference,
415 whereas Mus81-dependent class II COs are unchanged in *msh2Δ* (Cooper et al. 2018). *Sz. pombe*
416 operates only a class II CO pathway via Mus81-processing, completely lacking a class I CO pathway.
417 Nevertheless, the absence of Msh2 in fission yeast has a profound effect on CO frequency, and the
418 way recombination intermediates are processed (Figure 2).

419   FANCM- and RecQ-family DNA helicases/translocases are implicated in regulating meiotic
420 recombination outcome in several different organisms (Lorenz et al. 2012; Crismani et al. 2012; De
421 Muyt et al. 2012; Cromie, Hyppa, and Smith 2008; Hatkevich et al. 2017; Lukaszewicz, Howard-Till,
422 and Loidl 2013). In *Sz. pombe* Fml1 has been shown to specifically limit CO formation during the
423 late CO/NCO-decision (Lorenz et al. 2012). Fml1 acts as a promotor of NCOs, likely by driving late
424 recombination intermediates into the SDSA pathway, after strand invasion and DNA synthesis has
425 happened. In accordance with this, absence of *fml1* leads to an increase in CO among intragenic
426 *ade6⁺* events, but has little effect on intragenic recombination itself (Figure 3, Figure 3-figure
427 supplement 1) (Lorenz et al. 2012). This role is independent of the size of the intragenic interval, with
428 Fml1 driving 10-12% of NCO recombination in any case. The deletion of *rqh1* has a very strong
429 meiotic phenotype, leading to reductions in intragenic recombination, CO, and spore viability (Figure
430 3, Figure 3-figure supplement 1). This on its own would indicate an early role in promoting strand
431 exchange and/or DSB resection, but then Rqh1 is capable of promoting NCO formation among *ade6⁺*
432 events at some intragenic intervals (Figure 3, Figure 3-figure supplement 1). Most likely this is due
433 to Rqh1 actually performing the following functions: (I) promotion of interhomolog recombination
434 events, probably in cooperation with Rad55-57 and Rlp1-Rdl1-Sws1, but independently of Sfr1-Swi5
435 (Lorenz et al. 2014), potentially also by providing longer resection tracts (Osman et al. 2016); (II)

436   dismantling D-loops, this enables the release of break ends to search for homology elsewhere, starts
437   cycles of multiple consecutive invasion steps, and provides opportunities for Fml1 to drive NCO
438   formation via SDSA; and (III) branch migration of established D-loops and Holliday junctions, thereby
439   promoting heteroduplex DNA formation further away from the break site (Cromie, Hyppa, and Smith
440   2008).
441
442   **Environmental temperature influences recombination outcome**
443   The environmental temperature regime during crossing affects meiotic recombination outcome in
444   fission yeast, while DSB levels appear to be maintained across temperatures in the "fertile range"
445   (Figures 4, 5). Steps in the meiotic recombination pathway that are downstream of DSB formation,
446   such as strand resection and/or strand exchange are likely impaired at colder temperatures (Figure
447   6). Especially, intragenic recombination frequency shows strong changes with temperature within
448   the "fertile range", whereas overall COs and COs among intragenic events are less affected (Figure
449   4, Figure 4-figure supplement 1). Recombination monitored at non-hotspot alleles only are less
450   sensitive to temperature changes than those involving a hotspot (Supplementary File 1-Table S4);
451   this could be a manifestation of CO invariance suggested to explain a stronger drive towards
452   interhomolog recombination at non-hotspots (Hyppa and Smith 2010). CO changes over
453   temperature do definitely not follow a U-shape curve like in *Drosophila* or *Arabidopsis* (Plough 1917;
454   Lloyd et al. 2018), where CO recombination is highest at the more extreme temperatures within the
455   "fertile range". Similar to *C. elegans* (Rose and Baillie 1979) CO rates tend to be lower at low
456   temperatures (Figure 4-figure supplement 1). In *Hordeum vulgare* (barley) and *S. cerevisiae* CO
457   position, rather than overall frequency, changes with temperature (Higgins et al. 2012; Zhang et al.
458   2017). In *S. cerevisiae* this has largely been explained by differential activation of DSB hotspots at
459   different temperatures (Zhang et al. 2017). However, in contrast to *S. cerevisiae* where the location
460   of DSBs is maintained in only ~20% of cases between temperatures (14°C, 30°C, and 37°C) (Zhang
461   et al. 2017), in *Sz. pombe* this is true for ~70% of DSB sites (Hyppa et al. 2014). It is thus unlikely
462   that changes of recombination frequency due to differential hotspot activation over temperature is a
463   major contributing factor in *Sz. pombe*. Considering that overall CO frequency is only moderately
464   affected by temperature, whereas intragenic recombination rates change massively, a switch from
465   interhomolog to intersister recombination will unlikely be a key contributing factor, since this would
466   affect intergenic COs and intragenic recombination to an equal extent. Processes directly
467   downstream of DSB formation, such as strand invasion and stabilisation of strand exchange, are
468   temperature-sensitive (Figure 6), and are seemingly a major cause for low intragenic recombination
469   frequency at low temperatures.
470
471   **Concluding remarks**
472   Factors directly involved in generating CO and NCO recombinants during meiosis have been
473   identified and characterized in recent years (Osman et al. 2003; De Muyt et al. 2012; Lorenz et al.
474   2012; Lukaszewicz, Howard-Till, and Loidl 2013; Crismani et al. 2012), and several inroads have
475   been made in understanding how template choice is regulated and executed during meiotic
476   recombination in standard laboratory conditions (Hong et al. 2013; Lorenz et al. 2014). However, we
477   still only have a basic understanding of how underlying DNA sequence polymorphisms and
478   environmental parameters influence meiotic recombination outcomes. Here, we demonstrate that
479   specific DNA sequence differences between the two homologs strongly impact on which outcome is
480   achieved, and that this is largely driven by the action of the MutS-MutL complex. Other important
481   determinants influencing meiotic recombination outcome are environmental factors, such as
482   temperature. Temperature changes within the "fertile range" of a species grossly affects intra- and
483   intergenic recombination levels in several species (Plough 1917; Rose and Baillie 1979; Bomblies,
484   Higgins, and Yant 2015; Lloyd et al. 2018), likely by changing the positioning of the initial DSB
485   (Higgins et al. 2012; Zhang et al. 2017) and/or dynamics of DSB repair (Modliszewski et al. 2018;

11

486 this study). This highlights the importance of the interplay between intrinsic and environmental
487 parameters in shaping the genetic diversity of a given population.
488

Material and methods

490 **Bacterial and yeast strains and culture conditions**
491 *E. coli* strains were grown on LB and SOC media – where appropriate containing 100 µg/ml Ampicillin
492 (Sambrook and Russell 2000). Competent cells of *E. coli* strains NEB10®-beta (New England
493 BioLabs Inc., Ipswich, MA, USA), and XL1-blue (Agilent Technologies, Santa Clara, CA, USA) were
494 transformed following the protocols provided by the manufacturers. *Schizosaccharomyces pombe*
495 strains used for this study are listed in Supplementary File 2. Yeast cells were cultured on yeast
496 extract (YE), and on yeast nitrogen base glutamate (YNG) agar plates containing the required
497 supplements (concentration 250 mg/l on YE, 75 mg/l on YNG). Crosses were performed on malt
498 extract (ME) agar containing supplements at a final concentration of 50 mg/l (Sabatinos and
499 Forsburg 2010).

500 Different *ade6* hotspot and non-hotspot sequences (Figure 1-table supplement 2) were
501 introduced by crossing the respective mutant *ade6* strain with *ade6*+ strains carrying the *ura4*+ and
502 *his3*+ artificially introduced markers (aim) (UoA95, UoA96, UoA97, UoA98) (Osman et al. 2003). The
503 point mutations in the *ade6* alleles were verified by Sanger DNA sequencing (Source BioScience,
504 Nottingham, UK) (Figure 1-table supplement 2).

505 Using an established marker swap protocol (Sato, Dhut, and Toda 2005) the *natMX6*-marked
506 *rqh1Δ-G1* was derived from an existing *rqh1Δ::kanMX6* allele (Doe et al. 2002), creation of the
507 *natMX6*-marked *pms1-16* insertion mutant allele has been described previously (Lorenz 2015).

508 Marker cassettes to delete *msh3*, and *msh6*, and to partially delete *msh2* were constructed
509 by cloning targeting sequences of these genes into pFA6a-*kanMX6*, pAG25 (*natMX4*), and pAG32
510 (*hphMX4*), respectively, up- and downstream of the dominant drug resistance marker (Bähler et al.
511 1998; Goldstein and McCusker 1999). The targeting cassettes were released from the relevant
512 plasmids (pALo130, pALo132, pALo134) by a restriction digest, and transformed into the strains
513 FO652 (*msh2* and *msh6*) and ALP729 (*msh3*). For specifics of strain and plasmid construction
514 please refer to Supplementary File 3. Plasmid sequences are available on figshare
515 (https://figshare.com/s/ad72dbfe07a261fd4ee4). Epitope tagging of *hop1*+ with a C-terminal *13myc-*
516 *kanMX6* tag has been described in detail (Brown, Jarosinska, and Lorenz 2018).

517 Transformation of yeast strains was performed using an established lithium-acetate
518 procedure (Brown and Lorenz 2016). All plasmid constructs were verified by DNA sequencing
519 (Source BioScience plc, Nottingham, UK).

520 All DNA modifying enzymes (high-fidelity DNA polymerase Q5, restriction endonucleases,
521 T4 DNA ligase) were supplied by New England BioLabs. Oligonucleotides were obtained from
522 Sigma-Aldrich Co. (St. Louis, MO, USA).
523

524 **Genetic and cytological assays**
525 Determination of spore viability by random spore analysis and the meiotic recombination assay have
526 been previously described in detail (Osman et al. 2003; Sabatinos and Forsburg 2010).

527 Genomic DNA of Ade- Ura+ His+ progeny from an *ade6-3083×ade6-469* (ALP733×ALP731)
528 cross was used to PCR-amplify the *ade6* locus (oligonucleotides oUA219 5'-
529 AAAGTTGCATTTCACAATGC-3' and oUA66 5'-GTCTATGGTCGCCTATGC-3') for Sanger sequencing
530 (Eurofins Scientific, Brussels, Belgium) with oUA219, oUA66, or nested oligonucleotides oUA779 5'-
531 CTCATTAAGCTGAGCTGCC-3' and oUA780 5'-AAGCTCTCCATAGCAGCC-3'.

532 Meiotic time-courses and preparation of chromatin spreads were in essence performed as
533 described previously (Loidl and Lorenz 2009), except for the use of 100 mg/ml Lallzyme MMX
534 (Lallemand Inc., Montréal, Canada) as the only cell-wall digesting enzyme in the spheroplasting
535 solution of the chromatin spread protocol (Flor-Parra et al. 2014). Immunostaining was performed

12

536 according to an established protocol (Loidl and Lorenz 2009) using polyclonal rabbit α-myc (ab9106;
537 Abcam PLC, Cambridge, UK) at a 1:500 dilution and monoclonal rat α-GFP [3H9] (ChromoTek
538 GmbH, Planegg-Martinsried, Germany) at a 1:100 dilution as primary antibodies. Antibody-bound
539 protein was visualized using donkey α-rabbit IgG AlexaFluor-555 (ab150062; Abcam) and donkey
540 α-rat IgG AlexaFluor-488 (ab150153; Abcam), both at a 1:500 dilution, as secondary antibodies
541 conjugated to fluorophores. DNA was stained by Hoechst 33342 (Molecular Probes, Eugene, OR,
542 USA) at a final concentration of 1 μg/ml.
543　　　　Analysis was performed on a Zeiss Axio Imager.M2 (Carl Zeiss AG, Oberkochen, Germany)
544 epifluorescence microscope equipped with the appropriate filter sets to detect red, green, and blue
545 fluorescence. Black-and-white images were taken with a Zeiss AxioCam MRm CCD camera
546 controlled by AxioVision 40 software v4.8.2.0. Images were pseudo-coloured and overlayed using
547 Adobe Photoshop CC (Adobe Systems Inc., San José, CA, USA).
548　　　　For Rec7-GFP and Rad11-GFP focus counts, images of meiotic prophase I nuclei, as
549 identified by the presence of Hop1-13myc linear elements at the thread and network stages (Lorenz
550 et al. 2006), were captured as described using the above antibodies. Individual images were
551 acquired for each channel to detect Hop1-13myc, either Rec7-GFP or Rad11-GFP, and the DNA
552 stain Hoechst 33342. Single image channels were merged, and all GFP-positive foci counted within
553 the area defined by the Hoechst 33342 staining using the "count" function in Adobe Photoshop CC.
554

555 **Data presentation and Statistics**
556 Raw data is available on figshare (https://figshare.com/s/ad72dbfe07a261fd4ee4). Line graphs were
557 produced using Microsoft Excel 2016 (version 16.0.4638.1000, 32-bit), and scatter plots were
558 generated in GraphPad Prism 5 for Windows (version 5.04). Box-and-whisker plots were created in
559 R (version i386, 3.0.1) (http://www.r-project.org/) (Lorenz et al. 2014). R was also used to compute
560 Kruskal-Wallis test and Tukey's Honest Significant Differences employing the kruskal.test() and
561 TukeyHSD() functions, respectively. Mann-Whitney U tests were performed as previously described
562 (Lorenz et al. 2014).
563

564 # Acknowledgments
572

573 # Author contributions
574 SDB: conception and design, unpublished essential reagents (yeast strains, plasmids), acquisition
575 of data, analysis and interpretation of data, revising the manuscript; MNA, MJ, CA, SJM: acquisition
576 of data, revising the manuscript; MCW: analysis and interpretation of data, revising the manuscript;
577 AL: conception and design, unpublished essential reagents (yeast strains, plasmids), acquisition of
578 data, analysis and interpretation of data, drafting and revising the manuscript.
579

580
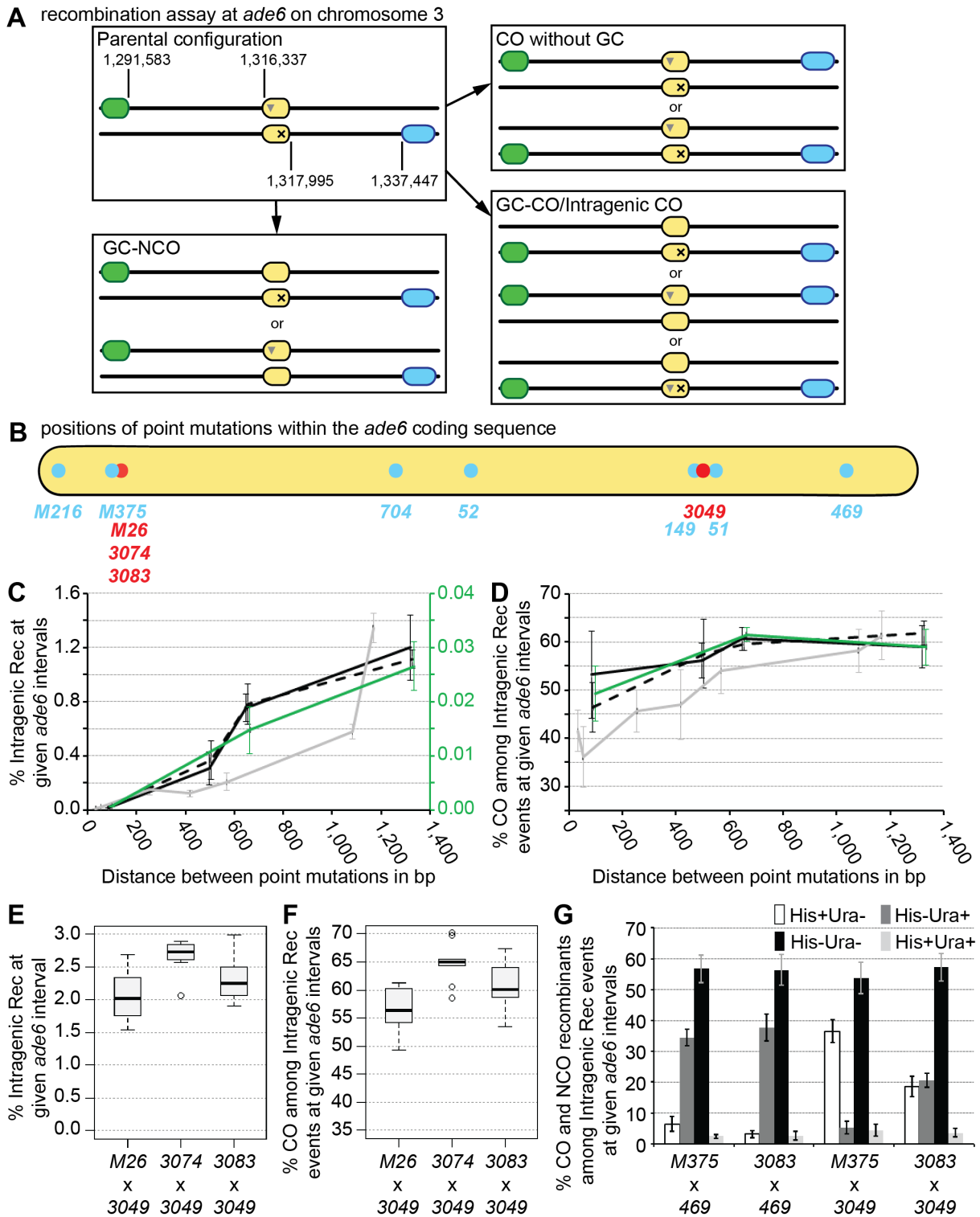
Figure 1. Physical distance between heteroalleles in *ade6* influences frequency of intragenic recombination (Intragenic Rec) and associated crossovers (COs). **(A)** Schematic showing the meiotic recombination assay at *ade6* (yellow) and its common outcomes. *ade6*+ recombinants can arise via gene conversion (GC) associated with a crossover (GC-CO) or a non-crossover (GC-NCO), alternatively intragenic COs can directly generate an *ade6*+ outcome. The positions of *ade6*, and the artificially introduced markers *his3*+-*aim* (light blue) and *ura4*+-*aim2* (green) on chromosome 3 are indicated [in bps]. Positions of point mutations are shown as ▼ and ×. **(B)** Schematic of the *ade6* coding sequence indicating the point mutations and their positions (approximately to scale) used in the recombination assays, hotspots are indicated in red, and non-hotspots in light blue. **(C)** Frequency of intragenic recombination and **(D)** frequency of CO among intragenic recombination events at *ade6* in wild type over distance between point mutations: crosses involving hotspot *ade6*-

593   *3083* as black solid line, UoA110×UoA100 (n=12), ALP733×UoA115 (n=12), ALP733×UoA119
594   (n=5), ALP733×ALP731 (n=20); crosses involving hotspot *ade6-3074* as black dashed line,
595   UoA106×UoA100 (n=12), UoA104×UoA115 (n=12), UoA104×UoA119 (n=6), UoA104×ALP731
596   (n=10); crosses involving hotspot *ade6-3049* as grey line, UoA122×UoA497 (n=6), UoA120×UoA463
597   (n=6),   UoA120×ALP731   (n=31),   UoA116×UoA123   (n=12),   UoA112×UoA123   (n=12),
598   ALP1541×UoA123 (n=12), UoA99×UoA123 (n=12); and crosses involving non-hotspot *ade6-M375*
599   as green line – needs to be read from the green secondary y-axis in (C)*,* UoA861×UoA100 (n=6),
600   ALP1541×UoA119 (n=6), ALP1541×ALP731 (n=16). **(E)** Frequency of intragenic recombination and
601   **(F)** frequency of CO among intragenic recombination events at *ade6* in wild type crosses involving
602   hotspot alleles only: FO1285×UoA123 (n=12), UoA104×UoA123 (n=9), and ALP733×UoA123 (n=9).
603   **(G)** Distribution of non-crossover (NCO) and crossover (CO) classes among intragenic
604   recombination events in wild type at *ade6*; ALP1541×ALP731 (n=16), ALP733×ALP731 (n=20),
605   ALP1541×UoA123 (n=12), ALP733×UoA123 (n=9). n indicates the number of independent crosses.
606   For details of data see Supplementary File 1-Table S1.
607

15
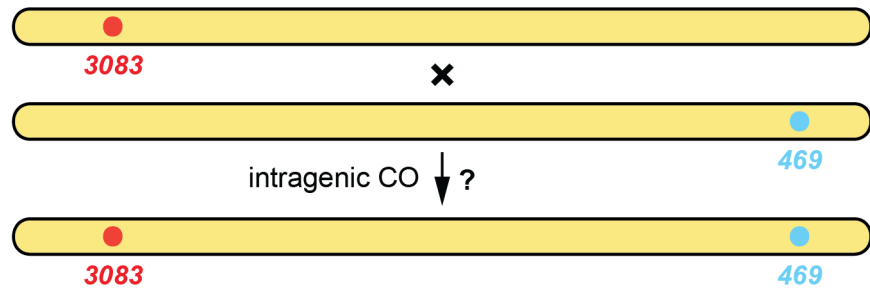
ade6 sequence of 32 Ade⁻ Ura⁺ His⁺ progeny from cross ALP733 (*ade6-3083*) × ALP731 (*ade6-469*)

colony number	5' end	3' end
1	*3083*	wt
2	wt	*469*
3	*3083*	wt
4	wt	*469*
5	wt	*469*
6	wt	*469*
7	wt	*469*
8	wt	469
9	wt	469
10	*3083*	wt
11	wt	469
12	wt	*469*
13	wt	469
* 14	*3083*	*469*
15	wt	469
16	*3083*	wt
17	wt	469
18	wt	469
19	*3083*	wt
* 20	*3083*	*469*
21	wt	469
22	*3083*	wt
23	wt	469
24	*3083*	wt
25	wt	469
26	*3083*	wt
27	*3083*	wt
28	wt	469
29	*3083*	wt
30	*3083*	wt
31	wt	469
32	wt	469

608
609 **Figure 1-figure supplement 1.** Intragenic COs between the *3083* and the *469* point mutations in
610 *ade6*. The *ade6* locus was sequenced in 32 Ade- Ura+ His+ colonies from an *ade6-3083×ade6-469*
611 (ALP733×ALP731) cross, in 2 instances (asterisks) it carried both mutations. wt (wild type), *3083*,
612 and *469* in bold indicate the status of the sequence confirmed by Sanger sequencing at the 5' and
613 3' ends, respectively. At the 3' end, the presence of 469 was assumed in some cases (not bold,
614 black) based on the colony being Ade⁻ and having a wt sequence at the 5' end.
615
616
617
618

16

619 **Figure 1-table supplement 2.** Sequence and position (counted from the A of the start codon ATG
620 as first position) of *ade6* point mutations (indicated in bold)

| allele	position	DNA sequence	reference
ade6-M216	G47A	ggtcaattgg**A**ccgaatgatg	(Szankasi et al. 1988)
ade6-M375	G133T	acaaattgat**T**gaggacgtga	(Szankasi et al. 1988)
ade6-M26	G136T	aattgatgga**T**gacgtgagca	(Szankasi et al. 1988)
ade6-3074	G136T/G142C	aattgatgga**T**gacgt**C**agcacattga	(Steiner and Smith 2005)
ade6-3083	A131G/G134T/G136T/G142C /G144T/A146G/A148C	aaattg**G**tg**T**a**T**gacgt**C**a**T**c**G**c**C**ttgatgc	(Steiner and Smith 2005)
ade6-704	T645A	ataatgtttg**A**catttagtat	(Park, Intine, and Maraia 2007)[a]
ade6-52	G796A	tttactcaac**A**aaattgctcc	(Steiner et al. 2009)[b]
ade6-149	C1181T	atcatgggtt**T**ggattctgat	(Schär and Kohli 1993)
ade6-3049	C1214A	aaagatgctg**A**cgtcatttta	(Steiner and Smith 2005)
ade6-51	C1267T	tgtttcagct**T**accgcacacc	(Schär, Munz, and Kohli 1993)
ade6-469	C1468T	tcagatgcct**T**gaggtgtccc	(Szankasi et al. 1988)

621 [a]previously estimated by positional mapping to be C846A (Schär and Kohli 1993); theoretically both, T645A and C846A, create a UGA
622 stop codon suppressible by *sup3-5* (Park, Intine, and Maraia 2007).
623 [b]previously reported as T956C (Schär, Munz, and Kohli 1993)
624
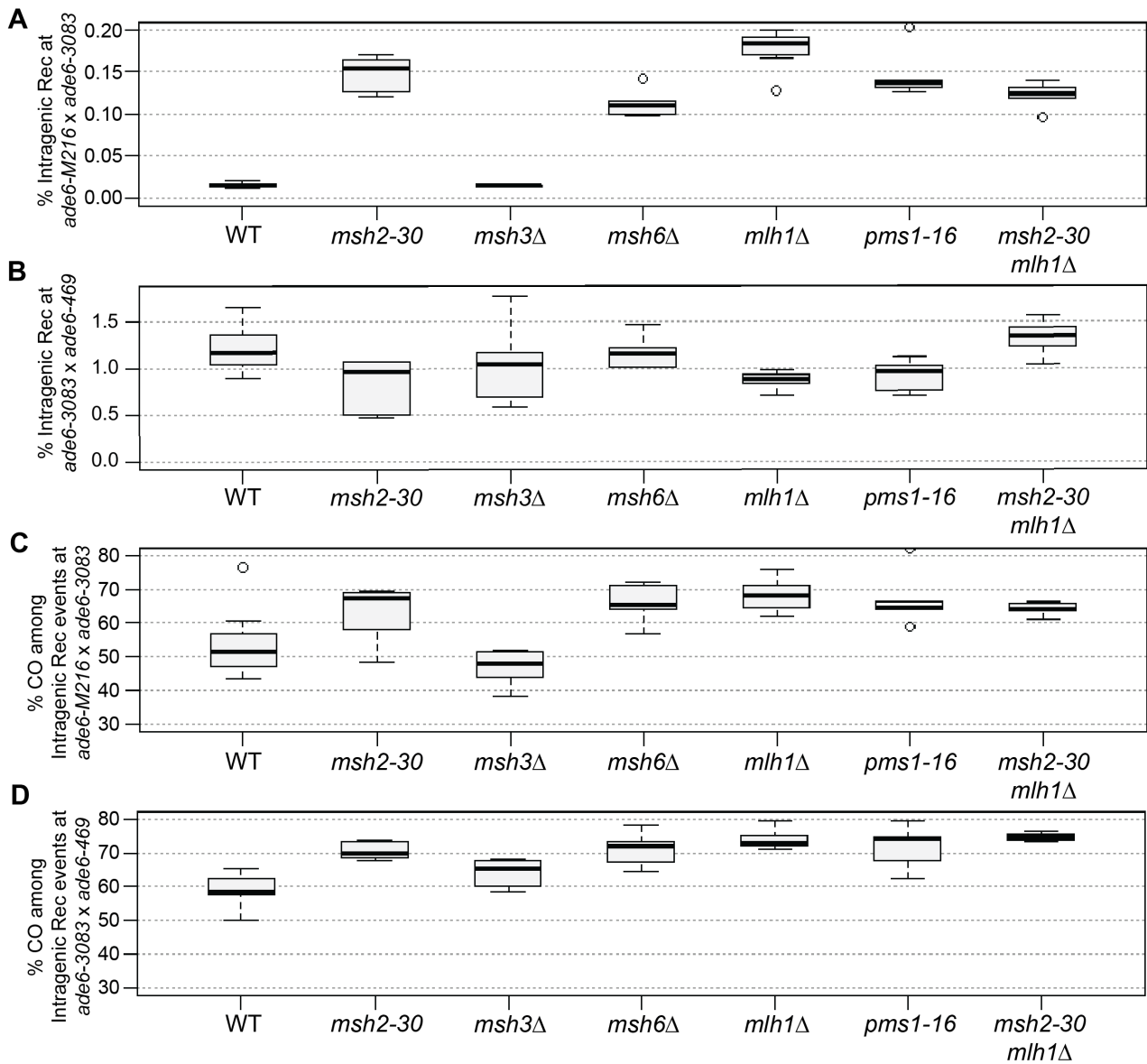
17

Figure 2. MutSα and MutLα, but not MutSβ, are major modulators of the intragenic recombination rate and the crossover (CO) frequency among intragenic recombination events. **(A, B)** Frequency of intragenic recombination (Intragenic Rec) in wild type (WT), *msh2*, *msh3*, *msh6*, *mlh1*, and *pms1* mutants **(A)** at the intragenic 85 bp interval *ade6-M216×ade6-3083*: UoA110×UoA100 (WT, n = 12), UoA478×UoA476 (*msh2-30*, n = 6), UoA494×UoA492 (*msh3Δ*, n = 6), UoA482×UoA480 (*msh6Δ*, n = 6), UoA364×UoA361 (*mlh1Δ*, n = 8), UoA407×UoA405 (*pms1-16*, n = 5), UoA828×UoA830 (*msh2-30 mlh1Δ*, n = 6); **(B)** at the intragenic 1,320 bp interval *ade6-3083×ade6-469*: ALP733×ALP731 (WT, n = 20), UoA477×UoA479 (*msh2-30*, n = 6), UoA493×UoA495 (*msh3Δ*, n = 6), UoA481×UoA483 (*msh6Δ*, n = 6), UoA362×UoA371 (*mlh1Δ*, n = 11), UoA406×UoA410 (*pms1-16*, n = 6), UoA827×UoA829 (*msh2-30 mlh1Δ*, n = 6). **(C, D)** Frequency of CO between *his3+-aim* and *ura4+-aim2* associated with intragenic recombination events at *ade6* in wild type (WT), *msh2*, *msh3*, *msh6*, *mlh1*, and *pms1* mutants **(C)** at the intragenic 85 bp interval *ade6-M216×ade6-3083*: strains as in (A); **(D)** at the intragenic 1,320 bp interval *ade6-3083×ade6-469*: strains as in (B). n indicates the number of independent crosses. For details of data see Supplementary File 1-Table S2.
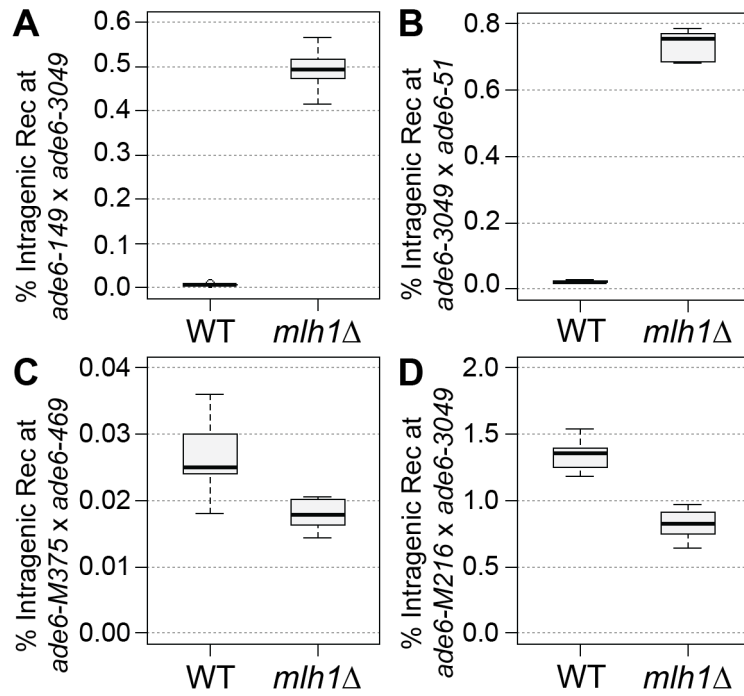
Figure 2-figure supplement 1. MutLα is a major modulator of intragenic recombination (Intragenic Rec) rate. Frequency of intragenic recombination in wild type (WT), and *mlh1Δ*. **(A)** at the intragenic 33 bp interval *ade6-149×ade6-3049*: UoA122×UoA497 (WT, n = 6), UoA368×UoA512 (*mlh1Δ*, n = 6); **(B)** at the intragenic 53 bp interval *ade6-3049×ade6-51*: UoA120×UoA463 (WT, n = 6), UoA366×UoA511 (*mlh1Δ*, n = 6); **(C)** at the intragenic 1,335 bp interval *ade6-M375×ade6-469*: ALP1541×ALP731 (WT, n = 16), UoA510×UoA371 (*mlh1Δ*, n = 6); **(D)** at the intragenic 1,168 bp interval *ade6-M216×ade6-3049*: UoA99×UoA123 (WT, n = 12), UoA368×UoA361 (*mlh1Δ*, n = 12); n indicates the number of independent crosses. For details of data see Supplementary File 1-Table S2.
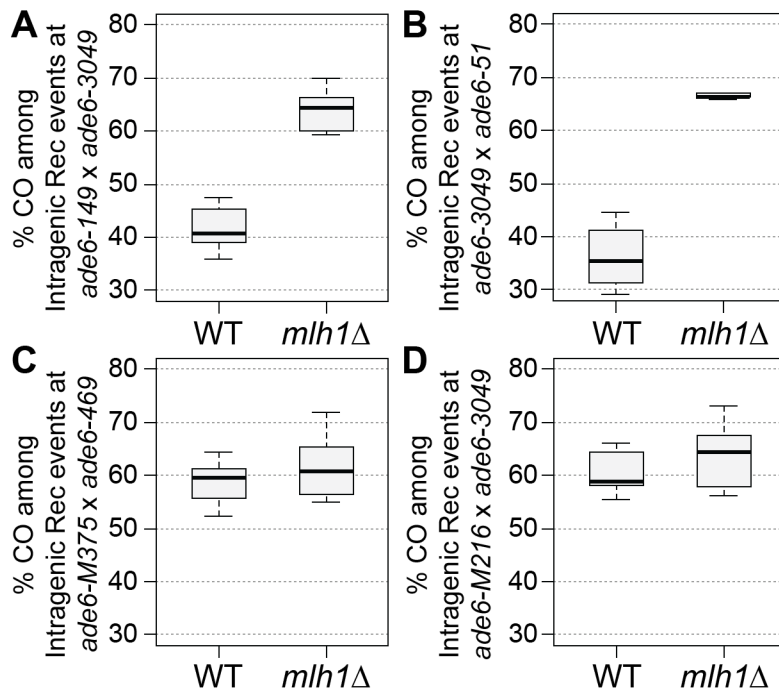

Figure 2-figure supplement 2. MutLα is a major modulator of crossover (CO) frequency among intragenic recombination (Intragenic Rec) events. Frequency of CO between *his3⁺-aim* and *ura4⁺-aim2* associated with intragenic recombination events at *ade6* in wild type (WT), and *mlh1Δ*. **(A)** at

19

657   the intragenic 33 bp interval *ade6-149×ade6-3049*: UoA122×UoA497 (WT, n = 6), UoA368×UoA512
658   (*mlh1Δ*, n = 6); **(B)** at the intragenic 53 bp interval *ade6-3049×ade6-51*: UoA120×UoA463 (WT, n =
659   6), UoA366×UoA511 (*mlh1Δ*, n = 6); **(C)** at the intragenic 1,335 bp interval *ade6-M375×ade6-469*:
660   ALP1541×ALP731 (WT, n = 16), UoA510×UoA371 (*mlh1Δ*, n = 6); **(D)** at the intragenic 1,168 bp
661   interval *ade6-M216×ade6-3049*: UoA99×UoA123 (WT, n = 12), UoA368×UoA361 (*mlh1Δ*, n = 12);
662   n indicates the number of independent crosses. For details of data see Supplementary File 1-Table
663   S2.
664
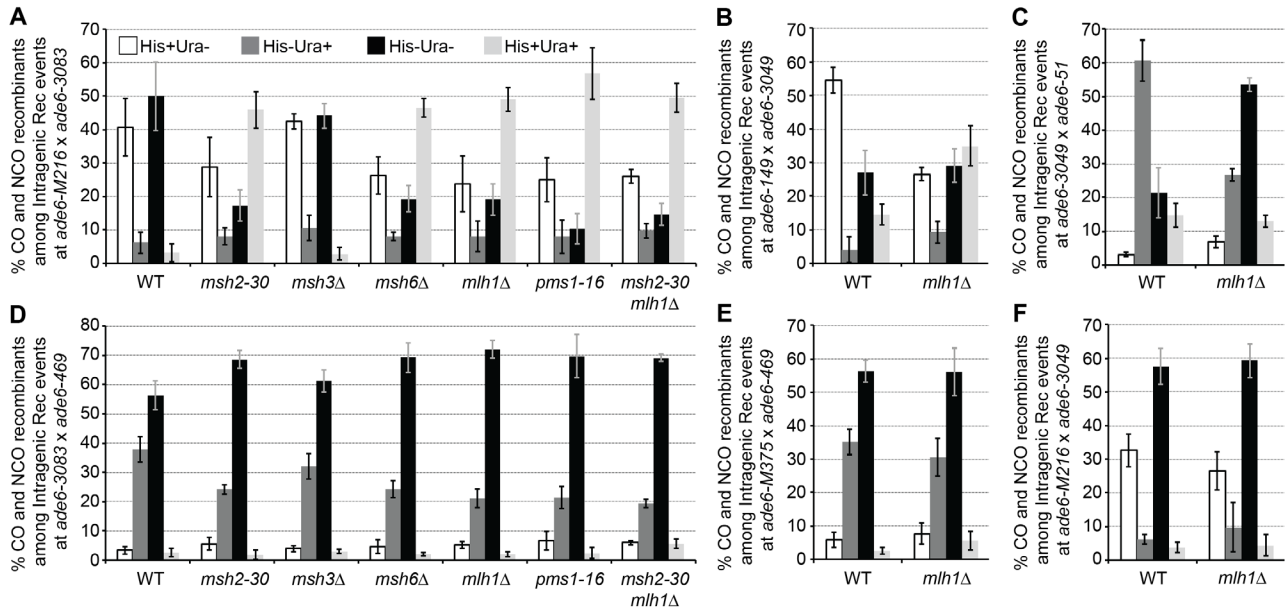
665
666   **Figure 2-figure supplement 3.** Distribution of non-crossover (NCO) and crossover (CO) classes
667   among intragenic recombination (Intragenic Rec) events at *ade6* in wild type (WT), *msh2*, *msh3*,
668   *msh6*, *mlh1*, and *pms1* mutants. **(A)** at the intragenic 85 bp interval *ade6-M216×ade6-3083*:
669   UoA110×UoA100 (WT, n = 12), UoA478×UoA476 (*msh2-30*, n = 6), UoA494×UoA492 (*msh3Δ*, n =
670   6), UoA482×UoA480 (*msh6Δ*, n = 6), UoA364×UoA361 (*mlh1Δ*, n = 8), UoA407×UoA405 (*pms1-16*,
671   n = 5), UoA828×UoA830 (*msh2-30 mlh1Δ*, n = 6); **(B)** at the intragenic 33 bp interval *ade6-149×ade6-*
672   *3049*: UoA122×UoA497 (WT, n = 6), UoA368×UoA512 (*mlh1Δ*, n = 6); **(C)** at the intragenic 53 bp
673   interval *ade6-3049×ade6-51*: UoA120×UoA463 (WT, n = 6), UoA366×UoA511 (*mlh1Δ*, n = 6); **(D)** at
674   the intragenic 1,320 bp interval *ade6-3083×ade6-469*: ALP733×ALP731 (WT, n = 20),
675   UoA477×UoA479 (*msh2-30*, n = 6), UoA493×UoA495 (*msh3Δ*, n = 6), UoA481×UoA483 (*msh6Δ*, n
676   = 6), UoA362×UoA371 (*mlh1Δ*, n = 11), UoA406×UoA410 (*pms1-16*, n = 6), UoA827×UoA829
677   (*msh2-30 mlh1Δ*, n = 6); **(E)** at the intragenic 1,335 bp interval *ade6-M375×ade6-469*:
678   ALP1541×ALP731 (WT, n = 16), UoA510×UoA371 (*mlh1Δ*, n = 6); **(F)** at the intragenic 1,168 bp
679   interval *ade6-M216×ade6-3049*: UoA99×UoA123 (WT, n = 12), UoA368×UoA361 (*mlh1Δ*, n = 12);
680   n indicates the number of independent crosses. For details of data see Supplementary File 1-Table
681   S2.
682
683
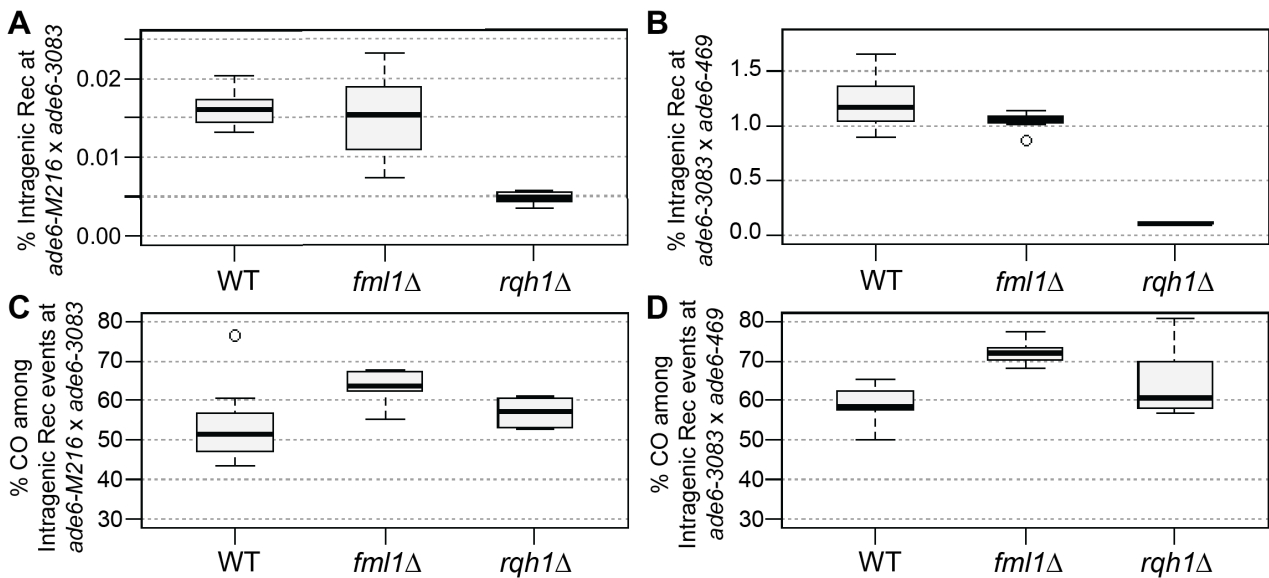
Figure 3. The RecQ-family helicase Rqh1, but not the FANCM-type helicase Fml1, is a major modulator of the intragenic recombination rate. Rqh1 and Fml1 are major modulators of crossover (CO) frequency among intragenic recombination events. Frequency of intragenic recombination (Intragenic Rec) in WT, *fml1*, and *rqh1* deletions **(A)** at the intragenic 85 bp interval *ade6-M216×ade6-3083*: UoA110×UoA100 (WT, n = 12), UoA450×UoA447 (*fml1Δ*, n = 9), UoA502×UoA499 (*rqh1Δ*, n = 6); **(B)** at the intragenic 1,320 bp interval *ade6-3083×ade6-469*: ALP733×ALP731 (WT, n = 20), ALP1133×MCW4718 (*fml1Δ*, n = 15), ALP781×ALP780 (*rqh1Δ*, n = 10). Frequency of CO between *his3+-aim* and *ura4+-aim2* associated with intragenic recombination events at *ade6* in WT, *fml1*, and *rqh1* deletions **(C)** at the intragenic 85 bp interval *ade6-M216×ade6-3083*: strains as in (A); **(D)** at the intragenic 1,320 bp interval *ade6-3083×ade6-469*: strains as in (B). n indicates the number of independent crosses. For details of data see Supplementary File 1-Table S2.
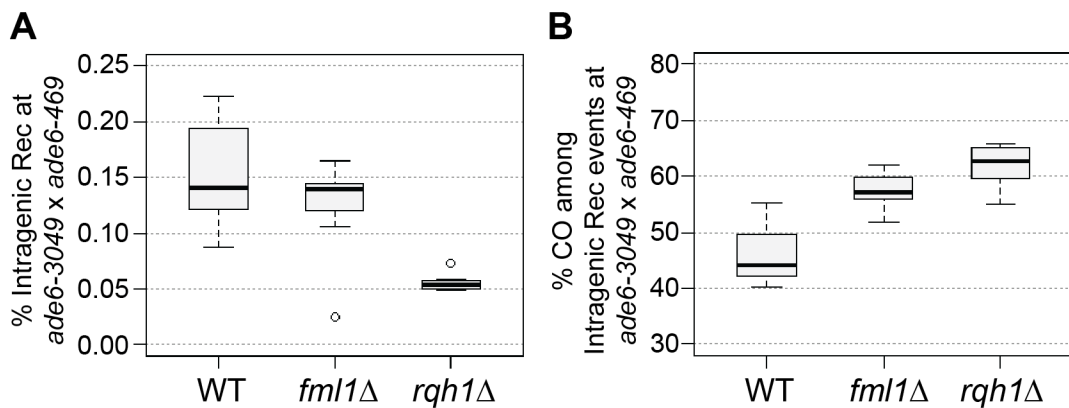
Figure 3-figure supplement 1. Rqh1 and Fml1 modulating meiotic recombination outcome at the intragenic 254 bp interval *ade6-3049×ade6-469*: **(A)** Frequency of intragenic recombination (Intragenic Rec) in wild type (WT), *fml1*, and *rqh1* mutants, UoA120×ALP731 (WT, n = 31), ALP1716×MCW4718 (*fml1Δ*, n = 11), MCW6587×ALP780 (*rqh1Δ*, n = 10); **(B)** Frequency of crossovers (CO) among intragenic recombination events at *ade6* in wild type (WT), *fml1*, and *rqh1* mutants, crosses as in (A). n indicates the number of independent crosses. For details of data see Supplementary File 1-Table S2.

708
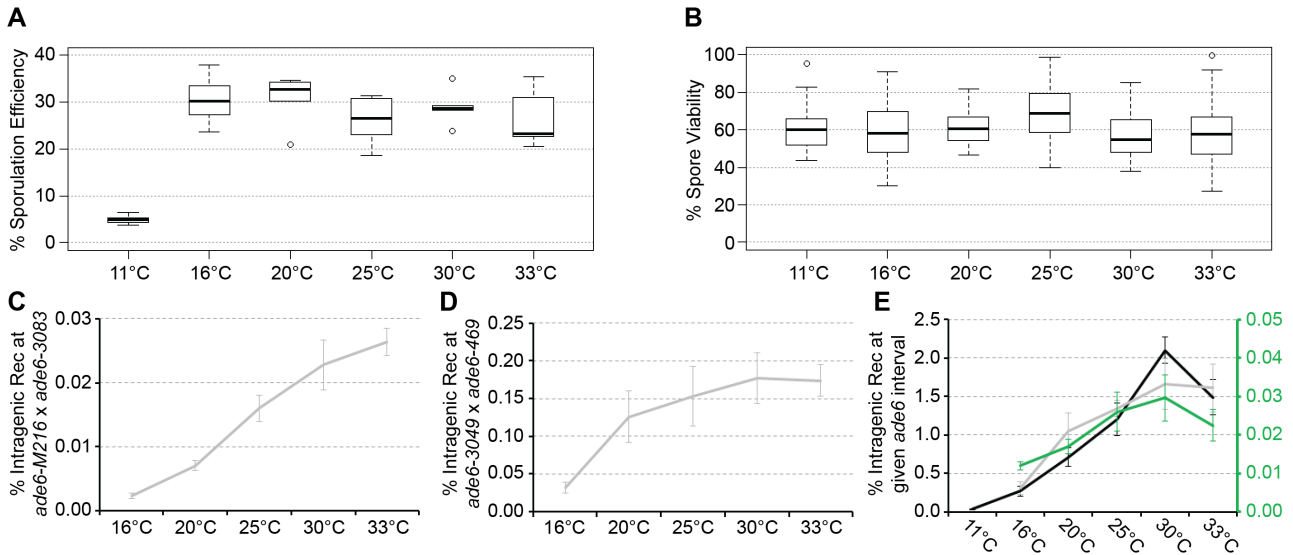
709
710 **Figure 4.** Environmental temperature alters intragenic recombination frequency at *ade6*. **(A)**
711 Sporulation efficiency in % determined in crosses of ALP714×ALP688 at 11°C after 14d (n = 7), at
712 16°C after 7d (n = 6), at 20°C after 5d (n = 5), at 25°C after 3d (n = 6), at 30°C after 2d (n = 6), and
713 at 33°C after 2d (n = 6). **(B)** Cumulative spore viability in % encompassing all data in (C – E) at 11°C
714 after 14d (n = 11), at 16°C after 7d (n = 64), at 20°C after 5d (n = 46), at 25°C after 3d (n = 75), at
715 30°C after 2d (n = 48), and at 33°C after 2d (n = 59). **(C – E)** Frequency of intragenic recombination
716 (Intragenic Rec) in wild type at the indicated intragenic *ade6* interval **(C)** UoA110×UoA100: 16°C (n
717 = 15), 20°C (n = 10), 25°C (n = 12), 30°C (n = 12), 33°C (n = 12); **(D)** UoA120×ALP731: 16°C (n =
718 8), 20°C (n = 8), 25°C (n = 31), 30°C (n = 8), 33°C (n = 8); **(E)** UoA99×UoA123 (*ade6-M216×ade6-*
719 *3049*, grey line): 16°C (n = 18), 20°C (n = 12), 25°C (n = 12), 30°C (n = 17), 33°C (n = 17);
720 ALP733×ALP731 (*ade6-3083×ade6-469*, black line): 11°C (n = 11), 16°C (n = 12), 20°C (n = 14),
721 25°C (n = 20), 30°C (n = 12), 33°C (n = 11); ALP1541×ALP731 (*ade6-M375×ade6-469*, green line
722 to be read from green secondary y-axis): 16°C (n = 12), 20°C (n = 12), 25°C (n = 16), 30°C (n = 12),
723 33°C (n = 11). n indicates the number of independent crosses. For details of data see Supplementary
724 File 1-Table S3 (A) and Supplementary File 1-Table S4 (B – E).
725
726

22

727
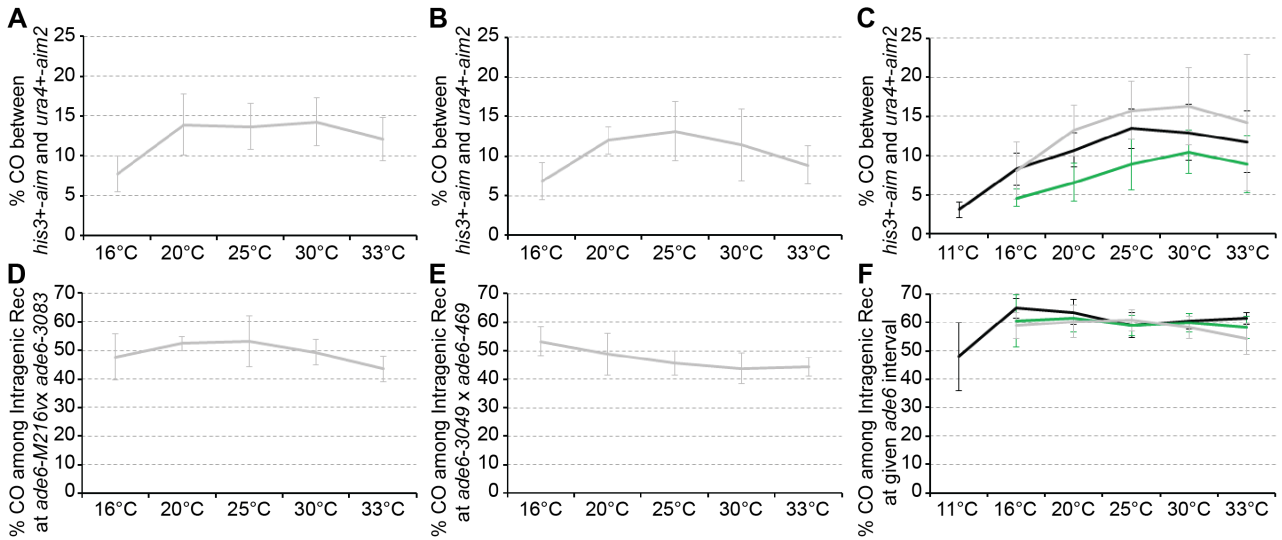
Figure 4-figure supplement 1. Frequency of **(A – C)** crossover (CO) between $his3^+$-aim and $ura4^+$-aim2, and **(D – F)** CO between $his3^+$-aim and $ura4^+$-aim2 among intragenic recombination (Intragenic Rec) events at ade6 from crosses performed at different temperatures. **(A, D)** UoA110×UoA100: 16°C (n = 15), 20°C (n = 10), 25°C (n = 12), 30°C (n = 12), 33°C (n = 12); **(B, E)** UoA120×ALP731: 16°C (n = 8), 20°C (n = 8), 25°C (n = 31), 30°C (n = 8), 33°C (n = 8); **(C, F)** UoA99×UoA123 (ade6-M216×ade6-3049, grey line): 16°C (n = 18), 20°C (n = 12), 25°C (n = 12), 30°C (n = 17), 33°C (n = 17); ALP733×ALP731 (ade6-3083×ade6-469, black line): 11°C (n = 11), 16°C (n = 12), 20°C (n = 14), 25°C (n = 20), 30°C (n = 12), 33°C (n = 11); ALP1541×ALP731 (ade6-M375×ade6-469, green line): 16°C (n = 12), 20°C (n = 12), 25°C (n = 16), 30°C (n = 12), 33°C (n = 11). n indicates the number of independent crosses. For details of data see Supplementary File 1-Table S4.

739

23
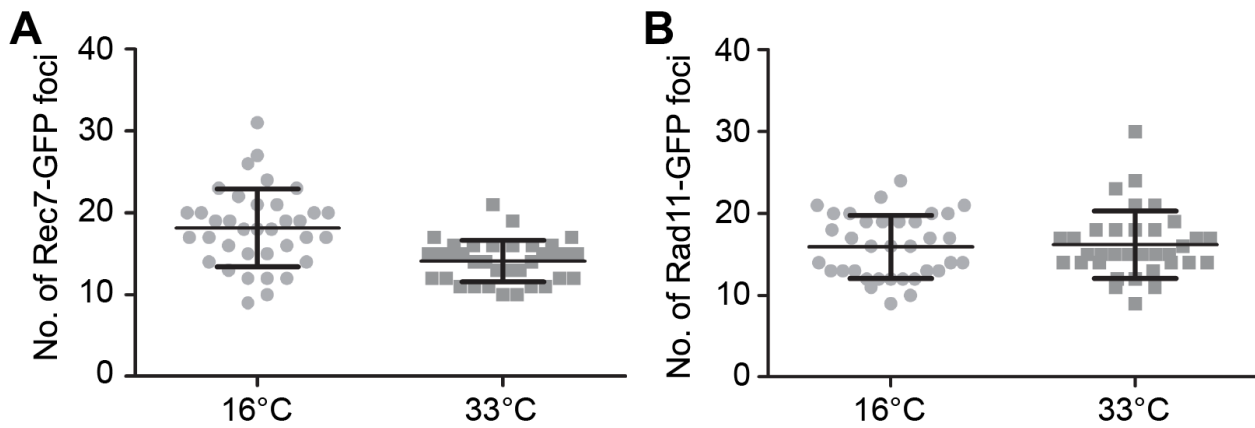
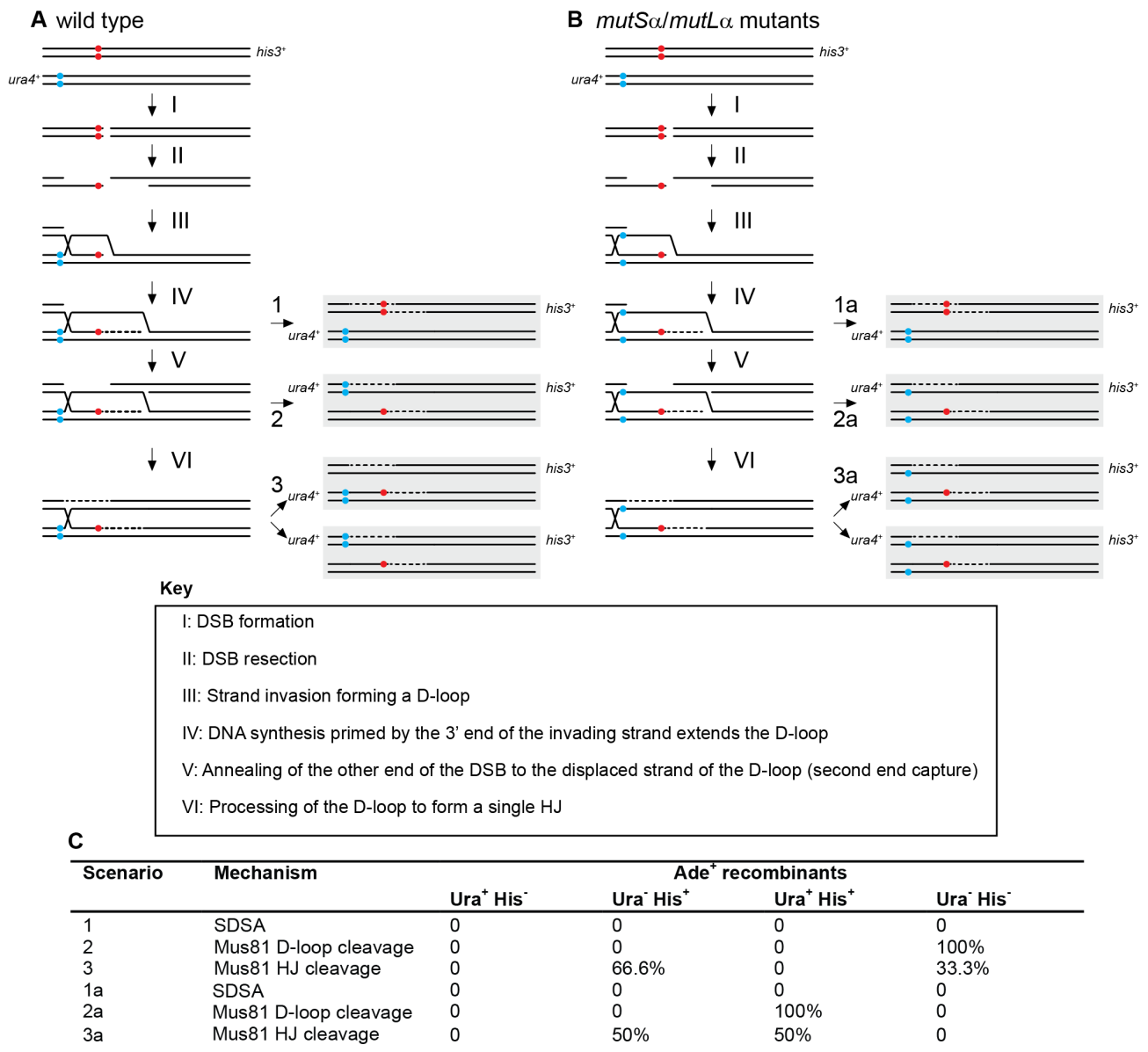**Figure 5.** DSB formation does not seem to be affected by temperature. **(A, B)** Focus counts of immune-detected Rec7-GFP and Rad11-GFP on Hop1-positive nuclear spreads from meiotic, azygotic timecourses at timepoints with maximum horsetail (meiotic prophase I) nucleus frequency; black horizontal lines indicate mean values, error bars represent standard deviation. **(A)** Number of Rec7-GFP foci per nucleus at 16°C (25hrs timepoint, n = 36) and 33°C (5hrs timepoint, n = 35) from meiotic timecourses of UoA825. **(B)** Number of Rad11-GFP foci per nucleus at 16°C (25hrs timepoint, n = 35) and 33°C (5hrs timepoint, n = 35) from meiotic timecourses of UoA826. For details of data see Supplementary File 1-Table S5.
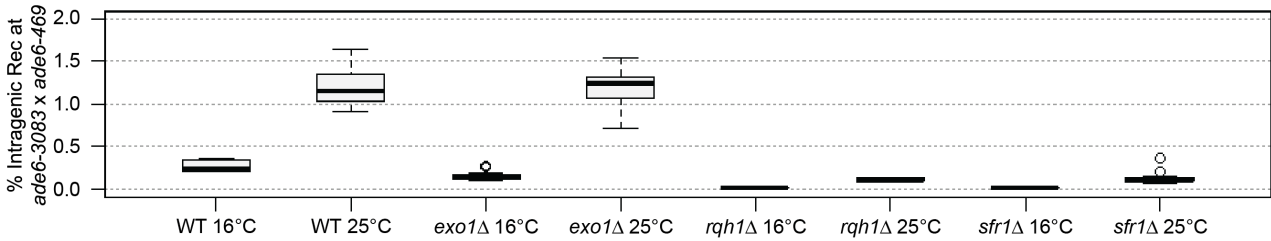
Figure 6. Cold temperature causes stronger reductions in intragenic recombination (Intragenic Rec) frequency in *exo1*, *rqh1*, or *sfr1* deletions than in wild type. Frequency of intragenic recombination (Intragenic Rec) at *ade6-3083×ade6-469* at 16°C and 25°C in wild type (WT), *exo1Δ*, *rqh1Δ*, and *sfr1Δ*. ALP733×ALP731 (WT; 16°C n = 12, 25°C n = 20), MCW4269×MCW4268 (*exo1Δ*; 16°C n = 11, 25°C n = 11), ALP781×ALP780 (*rqh1Δ*; 16°C n = 12, 25°C n = 10), ALP800×ALP782 (*sfr1Δ*; 16°C n = 11, 25°C n = 10). n indicates the number of independent crosses. For details of data see Supplementary File 1-Table S4.

Key

I: DSB formation

II: DSB resection

III: Strand invasion forming a D-loop

IV: DNA synthesis primed by the 3' end of the invading strand extends the D-loop

V: Annealing of the other end of the DSB to the displaced strand of the D-loop (second end capture)

VI: Processing of the D-loop to form a single HJ

C

Scenario	Mechanism	Ade$^+$ recombinants			
		Ura$^+$ His$^-$	Ura$^-$ His$^+$	Ura$^+$ His$^+$	Ura$^-$ His$^-$
1	SDSA	0	0	0	0
2	Mus81 D-loop cleavage	0	0	0	100%
3	Mus81 HJ cleavage	0	66.6%	0	33.3%
1a	SDSA	0	0	0	0
2a	Mus81 D-loop cleavage	0	0	100%	0
3a	Mus81 HJ cleavage	0	50%	50%	0

Figure 7. Possible scenarios for CO/NCO recombination events creating Ade$^+$ progeny from crosses with different *ade6* heteroalleles and *ura4$^+$-aim2* and *his3$^+$-aim* as flanking markers. **(A, B)** The two black lines represent double-stranded DNA of one chromatid; chromatids not involved in the depicted recombination event are omitted for clarity. Positions of the hotspot and non-hotspot alleles are indicated in red and light blue, respectively. **(A)** Predominant situation in wild type, where Ade$^+$ CO recombinants are mostly Ura$^-$ His$^-$. **(B)** Situation explaining the Ade$^+$ Ura$^+$ His$^+$ progeny observed in some *mutSα-mutLα* mutant crosses. Extensive branch migration and/or multiple invasion events could cause the D-loop or Holliday Junction (HJ) eventually being established upstream of the non-hotspot allele. Subsequent processing will generate Ade$^+$ Ura$^+$ His$^+$ CO progeny at a high frequency. **(C)** Frequency of possible recombination outcomes in crosses involving two *ade6* heteroalleles and flanking markers (*ura4$^+$-aim2* and *his3$^+$-aim*) as shown in (A) and (B).

25

References

Bähler, Jürg, Jian Qiu Wu, Mark S. Longtine, Nirav G. Shah, Amos McKenzie, Alexander B. Steever, Achim Wach, Peter Philippsen, and John R. Pringle. 1998. "Heterologous Modules for Efficient and Versatile PCR-Based Gene Targeting in *Schizosaccharomyces Pombe*." *Yeast* 14 (10): 943–51. doi:10.1002/(SICI)1097-0061(199807)14:10<943::AID-YEA292>3.0.CO;2-Y.

Bomblies, Kirsten, James D. Higgins, and Levi Yant. 2015. "Meiosis Evolves: Adaptation to External and Internal Environments." *New Phytologist* 208 (2): 306–23. doi:10.1111/nph.13499.

Börner, G Valentin, Nancy Kleckner, and Neil Hunter. 2004. "Crossover/Noncrossover Differentiation, Synaptonemal Complex Formation, and Regulatory Surveillance at the Leptotene/Zygotene Transition of Meiosis." *Cell* 117 (1): 29–45. http://www.ncbi.nlm.nih.gov/pubmed/15066280.

Brown, Simon D, and Alexander Lorenz. 2016. "Single-Step Marker Switching in *Schizosaccharomyces Pombe* Using a Lithium Acetate Transformation Protocol." *Bio-Protocol* 6 (24): e2075. doi:10.21769/BioProtoc.2075.

Brown, Simon David, Olga Dorota Jarosinska, and Alexander Lorenz. 2018. "Genetic Interactions between the Chromosome Axis-Associated Protein Hop1 and Homologous Recombination Determinants in Schizosaccharomyces Pombe." *Current Genetics* 64 (5): 1089–1104. doi:10.1007/s00294-018-0827-7.

Cooper, Tim J, Margaret R Crawford, Laura J Hunt, Marie-Claude Marsolier-Kergoat, Bertrand Llorente, and Matthew J Neale. 2018. "Mismatch Repair Impedes Meiotic Crossover Interference." *BioRxiv*, 480418. doi:10.1101/480418.

Crismani, Wayne, Chloé Girard, Nicole Froger, Mónica Pradillo, Juan Luis Santos, Liudmila Chelysheva, Gregory P. Copenhaver, Christine Horlow, and Raphaël Mercier. 2012. "FANCM Limits Meiotic Crossovers." *Science* 336 (6088): 1588–90. doi:10.1126/science.1220381.

Cromie, Gareth A, Randy W Hyppa, and Gerald R Smith. 2008. "The Fission Yeast BLM Homolog Rqh1 Promotes Meiotic Recombination." *Genetics* 179 (3): 1157–67. doi:10.1534/genetics.108.088955.

Cromie, Gareth A, Randy W Hyppa, Andrew F Taylor, Kseniya Zakharyevich, Neil Hunter, and Gerald R Smith. 2006. "Single Holliday Junctions Are Intermediates of Meiotic Recombination." *Cell* 127 (6): 1167–78. doi:10.1016/j.cell.2006.09.050.

Doe, Claudette L, Jong Sook Ahn, Julie Dixon, and Matthew C Whitby. 2002. "Mus81-Eme1 and Rqh1 Involvement in Processing Stalled and Collapsed Replication Forks." *The Journal of Biological Chemistry* 277 (36): 32753–59. doi:10.1074/jbc.M202120200.

Duroc, Yann, Rajeev Kumar, Lepakshi Ranjha, Céline Adam, Raphaël Guérois, Khan Md Muntaz, Marie-Claude Marsolier-Kergoat, et al. 2017. "Concerted Action of the MutLβ Heterodimer and Mer3 Helicase Regulates the Global Extent of Meiotic Gene Conversion." *ELife* 6: e21900. doi:10.7554/eLife.21900.

Farah, Joseph A, Gareth A Cromie, and Gerald R Smith. 2009. "Ctp1 and Exonuclease 1, Alternative Nucleases Regulated by the MRN Complex, Are Required for Efficient Meiotic Recombination." *Proceedings of the National Academy of Sciences of the United States of America* 106 (23): 9356–61. doi:10.1073/pnas.0902793106.

Flor-Parra, Ignacio, Jacob Zhurinsky, Manuel Bernal, Paola Gallardo, and Rafael R Daga. 2014. "A Lallzyme MMX-Based Rapid Method for Fission Yeast Protoplast Preparation." *Yeast (Chichester, England)* 31 (2): 61–66. doi:10.1002/yea.2994.

Fox, M E, J B Virgin, J Metzger, and G R Smith. 1997. "Position- and Orientation-Independent Activity of the *Schizosaccharomyces Pombe* Meiotic Recombination Hot Spot *M26*." *Proceedings of the National Academy of Sciences of the United States of America* 94 (14): 7446–51. doi:10.1073/pnas.94.14.7446.

828 Goldstein, A L, and J H McCusker. 1999. "Three New Dominant Drug Resistance Cassettes for
829   Gene Disruption in *Saccharomyces Cerevisiae*." *Yeast* 15 (14): 1541–53.
830   doi:10.1002/(SICI)1097-0061(199910)15:14<1541::AID-YEA476>3.0.CO;2-K.

831 Gutz, Herbert. 1971. "Site Specific Induction of Gene Conversion in *Schizosaccharomyces*
832   *Pombe*." *Genetics* 69 (3): 317–37. https://www.ncbi.nlm.nih.gov/pubmed/17248549.

833 Haruta, Nami, Yumiko Kurokawa, Yasuto Murayama, Yufuko Akamatsu, Satoru Unzai, Yasuhiro
834   Tsutsui, and Hiroshi Iwasaki. 2006. "The Swi5-Sfr1 Complex Stimulates Rhp51/Rad51- and
835   Dmc1-Mediated DNA Strand Exchange *in Vitro*." *Nature Structural & Molecular Biology* 13 (9):
836   823–30. doi:10.1038/nsmb1136.

837 Hatkevich, Talia, Kathryn P. Kohl, Susan McMahan, Michaelyn A. Hartmann, Andrew M. Williams,
838   and Jeff Sekelsky. 2017. "Bloom Syndrome Helicase Promotes Meiotic Crossover Patterning
839   and Homolog Disjunction." *Current Biology* 27 (1). Elsevier Ltd.: 96–102.
840   doi:10.1016/j.cub.2016.10.055.

841 Higgins, James D., Ruth M. Perry, Abdellah Barakate, Luke Ramsay, Robbie Waugh, Claire
842   Halpin, Susan J. Armstrong, and F. Chris H. Franklin. 2012. "Spatiotemporal Asymmetry of
843   the Meiotic Program Underlies the Predominantly Distal Distribution of Meiotic Crossovers in
844   Barley." *The Plant Cell* 24 (10): 4096–4109. doi:10.1105/tpc.112.102483.

845 Holliday, Robin. 2007. "A Mechanism for Gene Conversion in Fungi." *Genetical Research* 5 (5–6):
846   282–304. doi:10.1017/S0016672308009476.

847 Hong, Soogil, Youngjin Sung, Mi Yu, Minsu Lee, Nancy Kleckner, and Keun P. Kim. 2013. "The
848   Logic and Mechanism of Homologous Recombination Partner Choice." *Molecular Cell* 51 (4):
849   440–53. doi:10.1016/j.molcel.2013.08.008.

850 Humphryes, Neil, and Andreas Hochwagen. 2014. "A Non-Sister Act: Recombination Template
851   Choice during Meiosis." *Experimental Cell Research* 329 (1). Elsevier: 53–60.
852   doi:10.1016/j.yexcr.2014.08.024.

853 Hunter, Neil. 2015. "Meiotic Recombination: The Essence of Heredity." *Cold Spring Harbor
854   Perspectives in Biology* 7 (12): a016618. doi:10.1101/cshperspect.a016618.

855 Hyppa, Randy W., Kyle R. Fowler, Lubos Cipak, Juraj Gregan, and Gerald R. Smith. 2014. "DNA
856   Intermediates of Meiotic Recombination in Synchronous *S. Pombe* at Optimal Temperature."
857   *Nucleic Acids Research* 42 (1): 359–69. doi:10.1093/nar/gkt861.

858 Hyppa, Randy W, and Gerald R Smith. 2010. "Crossover Invariance Determined by Partner Choice
859   for Meiotic DNA Break Repair." *Cell* 142 (2): 243–55. doi:10.1016/j.cell.2010.05.041.

860 Jeffares, Daniel C. 2018. "The Natural Diversity and Ecology of Fission Yeast." *Yeast* 35 (3): 253–
861   60. doi:10.1002/yea.3293.

862 Kan, Fengling, Mari K Davidson, and Wayne P Wahls. 2011. "Meiotic Recombination Protein
863   Rec12: Functional Conservation, Crossover Homeostasis and Early Crossover/Non-
864   Crossover Decision." *Nucleic Acids Research* 39 (4): 1460–72. doi:10.1093/nar/gkq993.

865 Kon, N, M D Krawchuk, B G Warren, G R Smith, and W P Wahls. 1997. "Transcription Factor
866   Mts1/Mts2 (Atf1/Pcr1, Gad7/Pcr1) Activates the *M26* Meiotic Recombination Hotspot in
867   *Schizosaccharomyces Pombe*." *Proceedings of the National Academy of Sciences of the
868   United States of America* 94 (25): 13765–70. http://www.ncbi.nlm.nih.gov/pubmed/9391101.

869 Lam, Isabel, and Scott Keeney. 2015. "Mechanism and Regulation of Meiotic Recombination
870   Initiation." *Cold Spring Harbor Perspectives in Biology* 7 (1): a016634.
871   doi:10.1101/cshperspect.a016634.

872 Langerak, Petra, Eva Mejia-Ramirez, Oliver Limbo, and Paul Russell. 2011. "Release of Ku and
873   MRN from DNA Ends by Mre11 Nuclease Activity and Ctp1 Is Required for Homologous
874   Recombination Repair of Double-Strand Breaks." *PLoS Genetics* 7 (9): e1002271.
875   doi:10.1371/journal.pgen.1002271.

876 Liti, Gianni. 2015. "The Fascinating and Secret Wild Life of the Budding Yeast *S. Cerevisiae*." *ELife*
877   4: e05835. doi:10.7554/eLife.05835.

878 Lloyd, Andrew, Chris Morgan, Chris Franklin, and Kirsten Bomblies. 2018. "Plasticity of Meiotic
879   Recombination Rates in Response to Temperature in *Arabidopsis*." *Genetics* 208 (4): 1409–
880   20. doi:10.1534/genetics.117.300588.

881 Loidl, Josef, and Alexander Lorenz. 2009. "Analysis of *Schizosaccharomyces Pombe* Meiosis by
882   Nuclear Spreading." *Methods in Molecular Biology*, Methods in Molecular Biology, 558
883   (January). Totowa, NJ: Humana Press: 15–36. doi:10.1007/978-1-60761-103-5_2.

884 Lorenz, Alexander. 2015. "New Cassettes for Single-Step Drug Resistance and Prototrophic
885   Marker Switching in Fission Yeast." *Yeast* 32 (12): 703–10. doi:10.1002/yea.3097.

886 ———. 2017. "Modulation of Meiotic Homologous Recombination by DNA Helicases." *Yeast* 34
887   (5): 195–203. doi:10.1002/yea.3227.

888 Lorenz, Alexander, Anna Estreicher, Jürg Kohli, and Josef Loidl. 2006. "Meiotic Recombination
889   Proteins Localize to Linear Elements in *Schizosaccharomyces Pombe*." *Chromosoma* 115 (4):
890   330–40. doi:10.1007/s00412-006-0053-9.

891 Lorenz, Alexander, Alizée Mehats, Fekret Osman, and Matthew C Whitby. 2014. "Rad51/Dmc1
892   Paralogs and Mediators Oppose DNA Helicases to Limit Hybrid DNA Formation and Promote
893   Crossovers during Meiotic Recombination." *Nucleic Acids Research* 42 (22): 13723–35.
894   doi:10.1093/nar/gku1219.

895 Lorenz, Alexander, Fekret Osman, Weili Sun, Saikat Nandi, Roland Steinacher, and Matthew C
896   Whitby. 2012. "The Fission Yeast FANCM Ortholog Directs Non-Crossover Recombination
897   during Meiosis." *Science (New York, N.Y.)* 336 (6088): 1585–88.
898   doi:10.1126/science.1220111.

899 Lorenz, Alexander, Jennifer L Wells, David W Pryce, Maria Novatchkova, Frank Eisenhaber,
900   Ramsay J McFarlane, and Josef Loidl. 2004. "*S. Pombe* Meiotic Linear Elements Contain
901   Proteins Related to Synaptonemal Complex Components." *Journal of Cell Science* 117 (Pt
902   15): 3343–51. doi:10.1242/jcs.01203.

903 Lorenz, Alexander, Stephen C West, and Matthew C Whitby. 2010. "The Human Holliday Junction
904   Resolvase GEN1 Rescues the Meiotic Phenotype of a *Schizosaccharomyces Pombe Mus81*
905   Mutant." *Nucleic Acids Research* 38 (6): 1866–73. doi:10.1093/nar/gkp1179.

906 Lukaszewicz, Agnieszka, Rachel A Howard-Till, and Josef Loidl. 2013. "Mus81 Nuclease and Sgs1
907   Helicase Are Essential for Meiotic Recombination in a Protist Lacking a Synaptonemal
908   Complex." *Nucleic Acids Research* 41 (20): 9296–9309. doi:10.1093/nar/gkt703.

909 Manhart, Carol M., and Eric Alani. 2016. "Roles for Mismatch Repair Family Proteins in Promoting
910   Meiotic Crossing Over." *DNA Repair* 38 (February). Elsevier B.V.: 84–93.
911   doi:10.1016/j.dnarep.2015.11.024.

912 Marsolier-Kergoat, Marie Claude, Md Muntaz Khan, Jonathan Schott, Xuan Zhu, and Bertrand
913   Llorente. 2018. "Mechanistic View and Genetic Control of DNA Recombination during
914   Meiosis." *Molecular Cell* 70 (1). Elsevier Inc.: 9–20. doi:10.1016/j.molcel.2018.02.032.

915 Marti, Thomas M., Christophe Kunz, and Oliver Fleck. 2002. "DNA Mismatch Repair and Mutation
916   Avoidance Pathways." *Journal of Cellular Physiology* 191 (1): 28–41. doi:10.1002/jcp.10077.

917 Martini, Emmanuelle, Valérie Borde, Matthieu Legendre, Stéphane Audic, Béatrice Regnault,
918   Guillaume Soubigou, Bernard Dujon, and Bertrand Llorente. 2011. "Genome-Wide Analysis of
919   Heteroduplex DNA in Mismatch Repair-Deficient Yeast Cells Reveals Novel Properties of
920   Meiotic Recombination Pathways." *PLoS Genetics* 7 (9): e1002305.
921   doi:10.1371/journal.pgen.1002305.

922 Martini, Emmanuelle, Robert L Diaz, Neil Hunter, and Scott Keeney. 2006. "Crossover
923   Homeostasis in Yeast Meiosis." *Cell* 126 (2): 285–95. doi:10.1016/j.cell.2006.05.044.

924 Miyoshi, Tomoichiro, Masaru Ito, and Kunihiro Ohta. 2013. "Spatiotemporal Regulation of Meiotic
925   Recombination by Liaisonin." *Bioarchitecture* 3 (1): 20–24. doi:10.4161/bioa.23966.

926 Modliszewski, Jennifer L, Hongkuan Wang, Ashley R Albright, Scott M Lewis, Alexander R
927   Bennett, Jiyue Huang, Hong Ma, Yingxiang Wang, and Gregory P. Copenhaver. 2018.
928   "Elevated Temperature Increases Meiotic Crossover Frequency via the Interfering (Type I)

929   Pathway in *Arabidopsis Thaliana*." Edited by Gregory S. Barsh. *PLOS Genetics* 14 (5):
930   e1007384. doi:10.1371/journal.pgen.1007384.

931   Muyt, Arnaud De, Lea Jessop, Elizabeth Kolar, Anuradha Sourirajan, Jianhong Chen, Yaron
932   Dayani, and Michael Lichten. 2012. "BLM Helicase Ortholog Sgs1 Is a Central Regulator of
933   Meiotic Recombination Intermediate Metabolism." *Molecular Cell* 46 (1). Elsevier Inc.: 43–53.
934   doi:10.1016/j.molcel.2012.02.020.

935   Osman, Fekret, Jong Sook Ahn, Alexander Lorenz, and Matthew C. Whitby. 2016. "The RecQ
936   DNA Helicase Rqh1 Constrains Exonuclease 1-Dependent Recombination at Stalled
937   Replication Forks." *Scientific Reports* 6 (February): 22837. doi:10.1038/srep22837.

938   Osman, Fekret, Julie Dixon, Claudette L Doe, and Matthew C Whitby. 2003. "Generating
939   Crossovers by Resolution of Nicked Holliday Junctions: A Role for Mus81-Eme1 in Meiosis."
940   *Molecular Cell* 12 (3): 761–74. doi:10.1016/S1097-2765(03)00343-5.

941   Park, Jung-Min, Robert V Intine, and Richard J Maraia. 2007. "Mouse and Human La Proteins
942   Differ in Kinase Substrate Activity and Activation Mechanism for TRNA Processing." *Gene
943   Expression* 14 (2): 71–81. http://www.ncbi.nlm.nih.gov/pubmed/18257391.

944   Parker, A E, R K Clyne, A M Carr, and T J Kelly. 1997. "The *Schizosaccharomyces Pombe
945   Rad11*+ Gene Encodes the Large Subunit of Replication Protein A." *Molecular and Cellular
946   Biology* 17 (5): 2381–90. http://www.ncbi.nlm.nih.gov/pubmed/9111307.

947   Piazza, Aurèle, William Douglass Wright, and Wolf Dietrich Heyer. 2017. "Multi-Invasions Are
948   Recombination Byproducts That Induce Chromosomal Rearrangements." *Cell* 170 (4): 760–
949   73. doi:10.1016/j.cell.2017.06.052.

950   Plough, H. H. 1917. "The Effect of Temperature on Linkage in the Second Chromosome of
951   *Drosophila*." *Proceedings of the National Academy of Sciences of the United States of
952   America* 3 (9): 553–55. doi:10.1073/pnas.3.9.553.

953   Pryce, David W, Alexander Lorenz, Julia B Smirnova, Josef Loidl, and Ramsay J McFarlane. 2005.
954   "Differential Activation of *M26*-Containing Meiotic Recombination Hot Spots in
955   *Schizosaccharomyces Pombe*." *Genetics* 170 (1): 95–106. doi:10.1534/genetics.104.036301.

956   Rogacheva, Maria V., Carol M. Manhart, G. Chen, Alba Guarne, Jennifer Surtees, and Eric Alani.
957   2014. "Mlh1-Mlh3, a Meiotic Crossover and DNA Mismatch Repair Factor,Is a Msh2-Msh3-
958   Stimulated Endonuclease." *Journal of Biological Chemistry* 289 (9): 5664–73.
959   doi:10.1074/jbc.M113.534644.

960   Rose, A M, and D L Baillie. 1979. "The Effect of Temperature and Parental Age on Recombination
961   and Nondisjunction in *Caenorhabditis Elegans*." *Genetics* 92 (2): 409–18.

962   Sabatinos, Sarah A, and Susan L Forsburg. 2010. "Molecular Genetics of *Schizosaccharomyces
963   Pombe*." *Methods in Enzymology* 470 (10). Elsevier Inc: 759–95. doi:10.1016/S0076-
964   6879(10)70032-X.

965   Sambrook, J.F., and D.W. Russell. 2000. *Molecular Cloning: A Laboratory Manual*. 3rd ed. Cold
966   Spring Harbor: Cold Spring Harbor Laboratory Press.

967   Sato, Masamitsu, Susheela Dhut, and Takashi Toda. 2005. "New Drug-Resistant Cassettes for
968   Gene Disruption and Epitope Tagging in *Schizosaccharomyces Pombe*." *Yeast* 22 (7): 583–
969   91. doi:10.1002/yea.1233.

970   Schär, Primo, and Jürg Kohli. 1993. "Marker Effects of G to C Transversions on Intragenic
971   Recombination and Mismatch Repair in *Schizosaccharomyces Pombe*." *Genetics* 133 (4):
972   825–35. https://www.ncbi.nlm.nih.gov/pubmed/8462844.

973   Schär, Primo, Peter Munz, and Jürg Kohli. 1993. "Meiotic Mismatch Repair Quantified on the Basis
974   of Segregation Patterns in *Schizosaccharomyces Pombe*." *Genetics* 133 (4): 815–24.

975   Steiner, Walter W, and Gerald R Smith. 2005. "Optimizing the Nucleotide Sequence of a Meiotic
976   Recombination Hotspot in *Schizosaccharomyces Pombe*." *Genetics* 169 (4): 1973–83.
977   doi:10.1534/genetics.104.039230.

978   Steiner, Walter W, Estelle M Steiner, Angela R Girvin, and Lauren E Plewik. 2009. "Novel

Nucleotide Sequence Motifs That Produce Hotspots of Meiotic Recombination in *Schizosaccharomyces Pombe*." *Genetics* 182 (2): 459–69. doi:10.1534/genetics.109.101253.

Surtees, J. A., J. L. Argueso, and E. Alani. 2004. "Mismatch Repair Proteins: Key Regulators of Genetic Recombination." *Cytogenetic and Genome Research* 107 (3–4): 146–59. doi:10.1159/000080593.

Szankasi, Philippe, Wolf Dietrich Heyer, Peter Schuchert, and Jürg Kohli. 1988. "DNA Sequence Analysis of the *Ade6* Gene of *Schizosaccharomyces Pombe* - Wild-Type and Mutant Alleles Including the Recombination Hot Spot Allele *Ade6-M26*." *Journal of Molecular Biology* 204 (4): 917–25. doi:10.1016/0022-2836(88)90051-4.

Wahls, Wayne P., and Mari K. Davidson. 2012. "New Paradigms for Conserved, Multifactorial, Cis-Acting Regulation of Meiotic Recombination." *Nucleic Acids Research* 40 (20): 9983–89. doi:10.1093/nar/gks761.

Yamada, Shintaro, Kunihiro Ohta, and Takatomi Yamada. 2013. "Acetylated Histone H3K9 Is Associated with Meiotic Recombination Hotspots, and Plays a Role in Recombination Redundantly with Other Factors Including the H3K4 Methylase Set1 in Fission Yeast." *Nucleic Acids Research* 41 (6): 3504–17. doi:10.1093/nar/gkt049.

Yamada, Shintaro, Mika Okamura, Arisa Oda, Hiroshi Murakami, Kunihiro Ohta, and Takatomi Yamada. 2017. "Correlation of Meiotic DSB Formation and Transcription Initiation around Fission Yeast Recombination Hotspots." *Genetics* 206 (2): 801–9. doi:10.1534/genetics.116.197954.

Zahn-Zabal, Monique, and Jürg Kohli. 1996. "The Distance-Dependence of the Fission Yeast *Ade6-M26* Marker Effect in Two-Factor Crosses." *Current Genetics* 29 (6): 530–36. doi:10.1007/BF02426957.

Zhang, Ke, Xue-Chang Wu, Dao-Qiong Zheng, and Thomas D Petes. 2017. "Effects of Temperature on the Meiotic Recombination Landscape of the Yeast *Saccharomyces Cerevisiae*." *MBio* 8 (6): e02099-17. doi:10.1128/mBio.02099-17.